UNIVERSITY OF CALIFORNIA,

IRVINE

Intracellular Consequences of Mitochondrial Transplantation

DISSERTATION

Submitted in partial satisfaction of the requirements

for the degree of

DOCTOR OF PHILOSOPHY

in Biomedical Engineering

by

Paria Ali Pour

Ph.D. Qualifying Examination Committee:

Professor Arash Kheradvar, Chair

Professor M. Cristina Kenney

Professor Kyriacos Athanasiou

DEDICATION

To

My beloved family

who I am forever indebted to for their endless love and support.

TABLE OF CONTENTS

LIST OF FIGURES

LIST OF TABLES

ACKNOWLEDGEMNTS

I would like to express my deepest appreciation and gratitude to my PhD advisor, Professor Arash Kheradvar. I am grateful for all the support and guidance that I received from him over the past five years. I appreciate the intellectual freedom I was given on this new line of research we started exploring together on mitochondrial engineering. Prof. Kheradvar's patience, encouragement, and belief in me helped me push forward through the challenges and was instrumental in my professional development and helped shape me into the independent scientist I am today. I am also thankful for his enthusiasm about my project, his support for attending various conferences, and the countless letters of recommendation he provided on my behalf to nominate me for various awards and support me for academic opportunities.

My gratitude also goes to committee members, Professor Cristina Kenney and Professor Kyriacos Athanasiou for their interest in my work and agreeing to serve on my Dissertation Committee. I am grateful to Professor Kenney for warmly welcoming me to her laboratory to complete the bioenergetics studies of my dissertation and her invaluable insights on mitochondrial bioenergetics which was instrumental to our fruitful collaboration on investigating the bioenergetics consequences of mitochondrial transplantation. Prof. Kenney never hesitated to extend her support to me, be it through career advice, providing letters of reference on my behalf, and even offering me a post-doctoral position in her lab and I am extremely grateful for her continued support.

I would like to also thank Professor Marquis Vawter and Brandi Rollins for accepting our invitation to collaborate on conducting genomics studies post mitochondrial transplantation to investigate the (long-term) adoptability of mitochondria post-transplantation. I specifically thank Brandi for sharing her knowledge with me and assisting me with the sequencing study. While our joint efforts were abruptly interrupted by the campus closure caused by the COVID-19 pandemic, my hope is that we can finish these interesting studies when the campus re-opens.

Additionally, I thank Professor Babak Shahbaba for his advice on statistical analyses of our bioenergetics studies.

I would like to thank Prof. Michael Zaragoza, Prof. Michelle Digman, and Prof. Peter Burke who served on my qualifying exam committee in addition to Prof. Kheradvar, Prof. Kenney, and Prof. Athanasiou. I would like to also thank my preliminary exam committee chair, Prof. Elliot Botvinck and committee members Prof. Jared Haun and Prof. Gregory Brewer. I would like to specifically thank Prof. Elliot Botvinick who has been supportive and enthusiastic about my work and Prof. Gregory Brewer for his post-doctoral position offer.

I would like to thank all the faculty (Interim Director Christopher Hughes, Prof. Elliot Botvinick, Prof. Tim Downing, Prof. Anna Grosberg, and Prof. Wendy Liu) and staff (Ann Fain and Linda McCarthy) at the Edwards Lifesciences Center for advanced Cardiovascular Technology. I would like to specifically extend my gratitude to Prof. Downing, Prof. Liu and Prof. Grosberg. I thank Prof. Downing for allowing me to use their nanodrop instrument which allowed me to quantitate mitochondrial DNA and characterize its purity. Additionally, I am appreciative that they provided me with their human dermal fibroblast cells which I used for some of my experiments. I thank Prof. Liu for allowing me to use their plate reader to quantitate mitochondrial protein which was used

for normalization of bioenergetics studies raw data and to quantitate mitochondrial superoxide production. I thank Prof. Anna Grosberg for providing me with an experimental suggestion to validate the specificity of pHrodo Red SE, during my 2017 chalk talk at the Edwards Lifesciences Center for Advanced Cardiovascular Technology Heart-to-Heart Session. Additionally, I thank Linda McCarthy, who was the Core Lab manager at the Edwards Lifesciences Center for Advanced Cardiovascular Technology, for warmly welcoming me into the center back when I joined in 2015 and for her willingness to help; and I thank Ann Fain for her help with general inquiries and ensuring my success in the CARE program. I thank all the past and present members of Prof. Kheradvar's Research Group (KLAB), specifically Dr. Ramin Zareian, for his positivity and willingness to help. I also thank my colleagues at Liu lab (specifically Praveen Veerasubramanian), Downing Lab, CML Lab and BEAMS Lab at the Edwards Lifesciences Center. I would like to also thank Prof. Weian Zhao for providing me with their human Jurkat cells that I used for some of my studies.

I thank Marilyn Chwa from Prof. Kenney's Research Group (Mitochondrial Research Laboratory) for showing me how to use the seahorse metabolic flux analyzer which I used for my bioenergetics studies. I thank Agilent's Cell Analysis Team (particularly Courtney Nadeou Watts and Dr. Xiaofei Chen) for their valuable inputs related to bioenergetics studies and ThermoFisher Scientific Support Team for their assistance with the assays and kits used to conduct the studies detailed in this work. Furthermore, I thank UC Irvine's Optical Biology Core's manager, Dr. Adeela Syed, Couryn Beleck from Keyence Corportation Life Science Microscope Team, Matthew Bell from Nanolive Team, Andrew Brumm and Dr. Ram Stanciauskas from Nikon Team, and UC Irvine's Flow Core Facility manager, Dr. Jennifer Atwood, for their assistance in imaging aspects of the study.

Additionally, I would like to thank UCI's Henry Samueli School of Engineering director, Jean Bennet, and past assistant director, Connie Cheng, and Biomedical Engineering Department's past academic coordinator, Clare Cheng, and current academic coordinator, Maggie Mulcare for their support. I would like to also thank Dr. Sharnnia Artis, for her support and trust in me and giving me the opportunity to serve as a Diversity Ambassador for the School of Engineering. I enjoyed my interactions with the prospective graduate students admitted to the Biomedical Engineering Program (from disadvantaged socioeconomic or educational background) and answering their questions, and I am happy in doing so I contributed to enrollment of a more diverse graduate student population at UC Irvine.

I would like to also thank all my friends and classmates in the Biomedical Engineering Program and outside the Biomedical Engineering for their friendship and making the classes, seminars, clinical rotations, and graduate school, overall, a fun and fulfilling experience.

And last but certainly not least, I would like to thank my family. I am truly honored and blessed to have their love and support. My mother is one of my earliest inspirations to pursue a PhD and has continuously supported me in this path. My love for scientific research and teaching stemmed from seeing her interactions with her students as a Biochemistry Professor. My sister, Parastoo, who in addition to listening to my many stories about my work, like my mother did, also helped me with many aspects of my work and accompanied me many late nights when I was doing experiments. And of course, my father, the "bestest" of best friends who is not here to see his little

girl all grown up and getting her PhD. I could never thank him enough for everything he did for me and all he taught me; his early loss itself instilled one of the most important life lessons in me, to be grateful of the people and appreciative of the opportunities I have.

Additionally, I would like to acknowledge the funding I received from the Henry Samueli School of Engineering (HSSoE Fellowship, Pathway to PhD Fellowship, and Bridge Fellowship) and Edwards Lifesciences Center for Advanced Cardiovascular Technology (CARE NIH T-32 Fellowship, 2T32HL116270-06A1) in support of my doctoral work. Part of chapters 1 and 2 were previously published in the Journal of American Heart Association (JAHA) and is used with permission of the publisher under CC-BY-NC.

VITA

Paria Ali Pour

Education

University of California – Irvine, Irvine, CA

- **Ph.D. Candidate in Biomedical Engineering** 2020

  Dissertation Title: Intracellular Consequences of Mitochondrial Transplantation into Cardiomyocytes. Faculty Advisor: Prof. Arash Kheradvar

- **Master of Science in Biomedical Engineering** 2018
- **Bachelor of Science in Biochemistry & Molecular Biology** 2016
- **Bachelor of Art in History** 2016

  Honors Senior Thesis Title: Role of Ovol2A Protein in Pancreatic Cancer Pathogenesis. Faculty Advisor: Prof. Xing Dai. Campuswide Honors Program (CHP) Student

Professional Experiences

University of California – Irvine, Irvine, CA

- 10/2015 – 05/2020: Graduate Student Researcher and Safety Representative (KLAB), Edwards Lifesciences Center for Advanced Cardiovascular Technology (Mentor: Prof. Arash Kheradvar)
- 09/2012 – 08/2015: Undergraduate Student Researcher, Department of Biological Chemistry, UC Irvine School of Medicine (Mentor: Prof. Xing Dai)

Food and Drug Administration (FDA), Office of Regulatory Affairs, Irvine, CA

- 06/2016 09/2016: Student Trainee

Journal Publications

J2. **Ali Pour, P.**, Kenney MC., Kheradvar, A. Bioenergetics Consequences of Mitochondrial Transplantation in Cardiomyocytes*, Journal of American Heart Association (JAHA),* 2020. Apr 7; 9(7): e014501. doi:10.1161/JAHA.119.014501. Epub 2020 Mar 23.

J1. **Ali Pour, P.,** Xing, D., Role of Ovol2A in Pancreatic Cancer Pathogenesis. *University of California Irvine Journal of Undergraduate Research in the Biological Sciences,* 2015.

Patents

IP01. **Ali Pour P.** and Kheradvar A. Mitochondrial Transplantation To Alter Energy Metabolism, *U.S. patent (16/794115) pending.*

Peer Reviewed Conference Proceedings

C1. **Ali Pour P,** Kenney MC., Kheradvar A. Mitochondrial Transplantation into Cardiomyocytes Leads to Transient Enhanced Bioenergetics. *AHA 2019 Scientific Sessions,* November 16-18, Philadelphia, PA.

Conference Presentations

CP5. **Ali Pour P**, Kheradvar A. Quantification of Success of Mitochondrial Transplantation in Cardiomyocytes. *BMES 2019 Annual Scientific Meeting*, October 16-19, Philadelphia, PA.

CP4. **Ali Pour P**, Kheradvar A. Endosymbiosis-inspired Mitochondrial Transplantation into Cardiomyocytes. *NHLBI 2019 Mitochondrial Biology Symposium on Mitochondrial Networks and Energetics*, September 26-27, Bethesda, Maryland.

CP3. **Ali Pour P**, Kheradvar A. Feasibility of Transplantation of Non-Autologous Mitochondria into Cardiomyocyte. *BMES 2018 Annual Scientific Meeting*, October 17-20, Atlanta, GA.

CP2. **Ali Pour P**, Zareian R, and Kheradvar A. Mitochondrial Transplantation through Co-incubation into Cardiomyocyte. *BMES 2017 Annual Scientific Meeting*, October 11-14, Phoenix, AZ.

CP1. **Ali Pour P**, Dai X. Role of Ovol2A Protein in Pancreatic Cancer Pathogenesis. *Western Regional Honors Council, 43rd Annual Conference*, April 9-10, 2016, Riverside, CA.

Local Presentations

P7. BME Seminar Series, *Department of Biomedical Engineering, UC Irvine*, April 19, 2018, Irvine, CA.

P6. Poster Presentation, *Bench to Bedside Symposium, Gavin Herbert Eye Institute*, March 23, 2018, Irvine, CA.

P5. Chalk Talk, Heart-to-Heart Training Club, *Edwards Lifesciences Center for Advanced Cardiovascular Technology*, March 14, 2017, Irvine, CA.

P4. Oral Presentation, *Mitochondrial Special Interest Group, UC Irvine Center for Complex Biological Symptoms*, April 8, 2016, Irvine, CA.

P3. Oral Presentation, *Undergraduate Research Opportunities Program (UROP) 23rd Annual Symposium*, Irvine, CA, May 14, 2016, Irvine, CA.

P2. Poster Presentation, *Ayala School of Biological Sciences Undergraduate Research Symposium*, April 24, 2015, Irvine, CA.

P1. Oral Presentation, *Ayala School of Biological Sciences Undergraduate Research Symposium*, April 16, 2015, Irvine, CA.

Honors and Awards

Feb 2019	Semi-finalist, 2019 UCI Grad Slam (a UC systemwide competition that showcases and awards the best three-minute research presentations by graduate scholars) UCI, Irvine, CA
Dec 2018	Elevator Pitch Finalist, Graduate Professional Success for PhD and Postdocs in the Biomedical Sciences (GPS-BIOMED), The Cove at UCI Applied Innovation, Irvine, CA
Oct 2018 – Jun 2019	PhD Bridge Fellowship 2018-2019, UC Irvine Henry Samueli School of Engineering (HSSoE), UCI, Irvine, CA
Jul 2018 – Jun 2020	NIH T32 Cardiovascular Applied Research and Entrepreneurship (CARE) Training Fellowship, The Edwards Lifesciences Center for Advanced Cardiovascular Technology, UCI, Irvine, CA
May 2018	Award of Excellence in Pre-medical Education, Association of Professors and Scholars of Iranian Heritage (APSIH), UCLA, LA, CA

May 2018	Recognition of Achievement in Graduate Level Education, APSIH, UCLA, LA, CA
Oct 2016 – Jun 2017	Engineering Pathway to the PhD Fellowship, HSSoE,UCI, Irvine, CA
Apr 2016 – Sep 2016	HSSoE Research Fellowship, UCI, Irvine, CA
Jan 2016	UC Irvine Biomedical Engineering Accelerated Graduate Admission Status, UCI, Irvine, CA
Oct 2015 – Jun 2016	UCI Undergraduate Research Opportunities (UROP) grant: "Studying the Mitochondria's Role in Cardiomyocytes' Performance through Mitochondrial Transplantation" under mentorship of Prof. Arash Kheradvar, UCI, Irvine, CA
Jun 2015 – Aug 2015	UCI Summer Undergraduate Research Program (SURP) grant: "Studying the Role of Ovol2A Protein in Pancreatic Cancer Pathogenesis Using a Knock-down System" under mentorship of Prof. Xing Dai, UCI, Irvine, CA
May 2015	Excellence in Research Award, UC Irvine School of Biological Sciences, UCI, Irvine, CA
May 2015	Howard B. Lawson Endowed Memorial Scholarship (for leadership, service, and significant contributions), UCI, Irvine, CA
Sep 2012 – Jun 2016	UC Irvine Campuswide Honors Program Student, UCI, Irvine, CA

Teaching Experiences

2017– 2019 Graduate Teaching Assistant, UCI, Irvine, CA

- BME 50B: Cell & Molecular Engineering
- Bio Sci 99: Molecular Biology
- Bio Sci 98: Biochemistry
- Bio Sci 97: Genetics
- Bio Sci 94: Organisms to Ecosystems
- Bio Sci 93: DNA to Organisms

2015 – 2016 Persian Language Instructor and Mentor, UCI, Irvine, CA

- Persian 10A: Persian Peer-to-Peer Language Mentor Program

University Service

Jan 2019 – May 2020	Engineering Diversity Ambassador (2019 & 2020), UCI, Irvine, CA
Apr 2016	Invited Speaker, UC Irvine's Biomedical Engineering Society's Spring Research Symposium, UCI, Irvine, CA
Sep 2014 – Mar 2015	Delivery of Care Volunteer, Gottschalk Medical Plaza, UC Irvine Health

Educational Outreach

Jun 2018	Volunteer Speaker, Turtle Rock Elementary School, Irvine, CA
Feb 2017	Competition Judge, Samueli Academy High School, Santa Ana, CA

Leadership Experiences

2013 – 2016	Founder and Co-President of Persian Language & Culture Club, UCI
2012 – 2013	Membership Chair of Iranian Education Fund, UCI

ABSTRACT OF THE DISERTATION

Intracellular Consequences of Mitochondrial Transplantation

By

Paria Ali Pour

Doctor of Philosophy in Biomedical Engineering

University of California, Irvine, 2020

Professor Arash Kheradvar, Chair

Mitochondrion is a membrane-enclosed organelle found in most eukaryotic cells, which plays a vital role in cellular metabolism and homeostasis. As the powerhouse of the cell, the clinical manifestations of mitochondrial damage and dysfunction are devastating. While there has been much new interest and research on therapies involving mitochondria to mitigate diseases ranging from cancer and cardiovascular diseases to neurodegenerative diseases such as Parkinson and Alzheimer, the intracellular consequences of mitochondrial transplantation are not well-studied or well-understood.

In this work, we show that autologous, non-autologus, and interspecies mitochondrial transplantation are feasible using a variety of microscopy technique. Moreover, we show that non-autologous transplantation of healthy mitochondria from skeletal muscle cells into normal cardiomyocytes leads to improved bioenergetics acutely. Using a metabolic flux analyzer, we measured the oxygen consumption rate (OCR) and extracellular acidification rate (ECAR), after sequential treatment with Oligomycin, FCCP, Rotenone/Antimycin A post-transplantation, and

compared the values to the control groups with no transplantation event at four time points of post 2-day, 7-day, 14-day , and 28-day. Compared to the control, we observed a statistically significant improvement in basal respiration and ATP production 48-hour post-transplantation. Maximal respiration and spare respiratory capacity were also enhanced post 48-hour, although not statistically significantly. With respect to the long-term studies, these levels returned to that of the control group. Our findings demonstrate the acute positive bioenergetics outcome of mitochondrial transplantation in normal cardiomyocytes, which appears to diminish in long-term.

This work delineates the potential of mitochondrial transplantation for clinical application in settings where there is an acute stress that would benefit from a boost in cellular bioenergetics. Given the observed bioenergetic profile of mitochondrial transplantation in normal cells, one of the remaining questions is whether the post-transplantation bioenergetics profile will be any different in cells with mitochondrial dysfunction. Future studies are crucial in determining the possible advantages of mitochondrial transplantation, if any, in mitigating mitochondrial diseases and other mitochondrial dysfunctions, as a cellular biotherapy.

CHAPTER 1: MITOCHONDRIAL BIOLOGY, MITOCHONDRIAL DISEASES, and MITOCHONDRIAL ENGINEERING

1.1 MITOCHONDRIAL ORIGIN AND BIOLOGY

The mitochondrion found in most eukaryotic cells provides nearly all of the cell's energy by the oxidative phosphorylation process through the mitochondrial respiratory chain [7, 8]. The eukaryotes' mitochondrion is believed to have evolved from a small, autotrophic bacterium that was engulfed by a larger primitive, heterotrophic, eukaryotic cell [8]. Owing to its origin, mitochondrion has a (maternally inherited [9]) genome that is distinct from the cell's nuclear

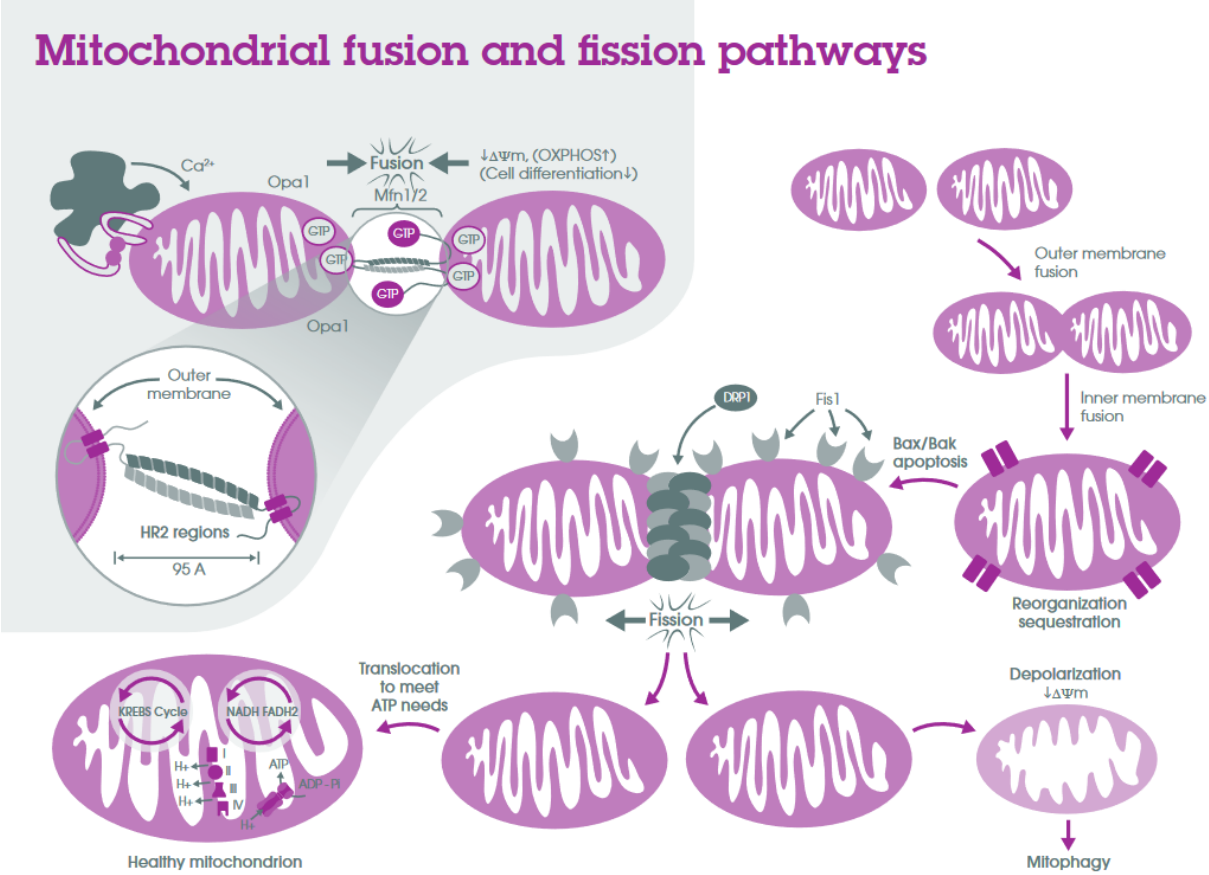

Fig. 1.1 | Mitochondrial Dynamics. Although mitochondria lack true DNA repair mechanisms, they use fission and fusion processes to maintain a healthy network. Fusion is the process in which two mitochondria fuse together and is accompanied by an increase in mitochondrial mass, which allows for complementation of mtDNA defects. Fission is the reverse process, in which the mitochondria undergo a division, accompanied by a decrease in mitochondrial mass, which allows for segregation of mitochondrial defects and degradation through mitophagy. Adapted from [2].

genome. Although mitochondrion was once a free-living organism, through the time and because of its symbiotic relationship, some of its genome has been translocated to the cell nucleus, making it an intracellular organelle dependent on the nucleus [3]. Like the nuclear genome, mitochondrial DNA (mtDNA) is constantly prone to damage and mutations. However, mitochondria lack effective DNA repair mechanisms so the mtDNA defects often clonally accumulate in subsequent mitochondria. Fission and Fusion dynamics are the processes that allow mitochondria to keep a healthy network, either complement mtDNA defects through fusion or degrade defective mitochondria through fission [10] (Fig. 1.1).

1.2 MITOCHONDRIAL DISORDERS AND DYSFUNCTIONS

Mitochondrial diseases develop as a result of a defective respiratory chain due to mutations in the nuclear DNA (nDNA) or mitochondrial DNA (mtDNA), as shown in Fig. 1.2. Regardless, the phenotypic representations of all mitochondrial disorders are deficiencies in energy metabolism and cell function with cardiac involvement as a common manifestation ranging from cardiomyopathy to arrhythmias and heart failure [8, 11, 12]. Furthermore, mitochondrial disease is multi-systematic and constitutes a large group of disorders. The combined results of the epidemiological data on childhood and adult mitochondrial disease, suggests for every 5,000 births in the U.S., one individual has an inherited mitochondrial disease, which is most likely an

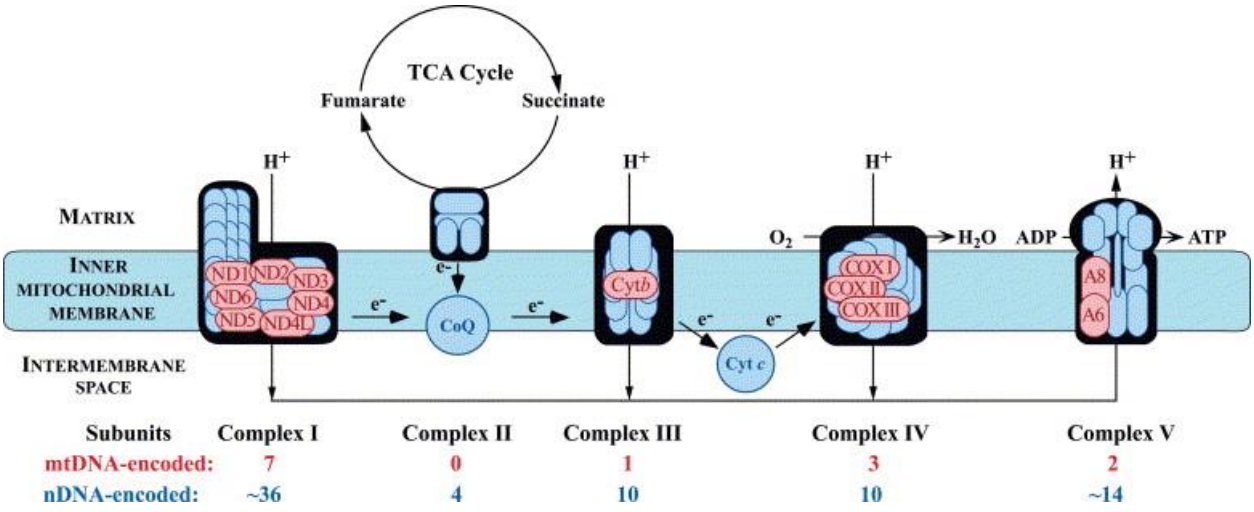

Fig. 1.2 | Mitochondrial Respiratory Chain. Mitochondrial diseases can be caused due to mutations in both mitochondrial DNA (mtDNA) and nuclear DNA (nDNA) since mitochondria is semi-autonomous and relies on nucleus to encode some of its proteins. Adapted from [3].

underestimate [11]. Mitochondrial diseases are complex diseases (Fig 1.3), in which patients present with multiple symptoms in different tissues and organs [11]. This complexity leads to the frequent poor diagnosis or misdiagnosis of this condition. No therapies are available for mitochondrial diseases, and the treatment continues to be mostly symptomatic, which does not appreciably change the course of the disease. The medication is limited to use of a mitochondrial cocktail composed of respiratory chain cofactors (Coenzyme Q10, L-carnitine, creatine, and L-

arginine) and antioxidants (thiamine, riboflavin, vitamin C and E, idebenon, and dihydrilipocate), which can only control the disease to some extent [12].

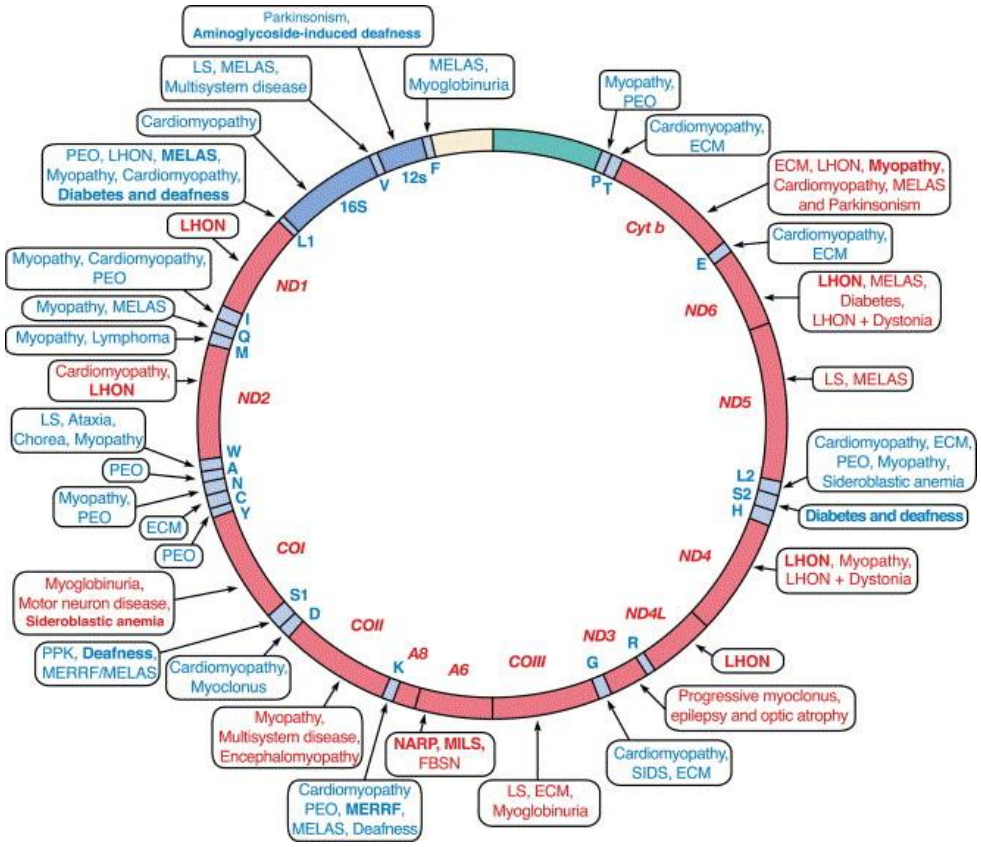

Fig. 1.3 | Mitochondria genome defects and Mitochondrial dysfunction. Human mitochondrial genome and the respective mitochondrial disorders caused by mutations in mitochondrial subunits. Adapted from [3].

1.3 OUR MITOCHONDRIAL ENGINEERING APPROACH

Inspired by mitochondria's endosymbiotic origin and the fact that mitochondrial diseases only present when the tissue specific threshold for mutations surpasses, we hypothesized that through transfer of whole intact functional mitochondrial organelle into cells with dysfunctional mitochondria we can modulate cellular bioenergetics and restore homeostasis to cells and consequently alleviate or eliminiate the clinical presentations of mitochondrial dysfunction.

1.4 OTHER MITOCHONDRIAL ENGINEERING APPORACHES

While there has not been much progress in finding a cure or therapy for mitochondrial diseases since they were clinically and genetically described about three decades ago, exciting advancements have been made in the field in the past few years. I will highlight some of these new approaches that have been recently developed or are underdevelopment briefly before discussing our work.

Recently, much interest has been devoted to cellular biotherapies involving mitochondria. Elliot et al. have successfully demonstrated that the introduction of normal mitochondria into human breast cancer cells restores mitochondrial function, inhibits cancer cell proliferation, and reverses chemoresistance by increasing the sensitivity of cells to breast cancer medication [13]. Regarding mitochondrial diseases, in 2017, early clinical feasibility of mitochondrial replacement therapy (MRT) in human has provided hope to mitigating inherited mitochondrial disorders [14]. The recent

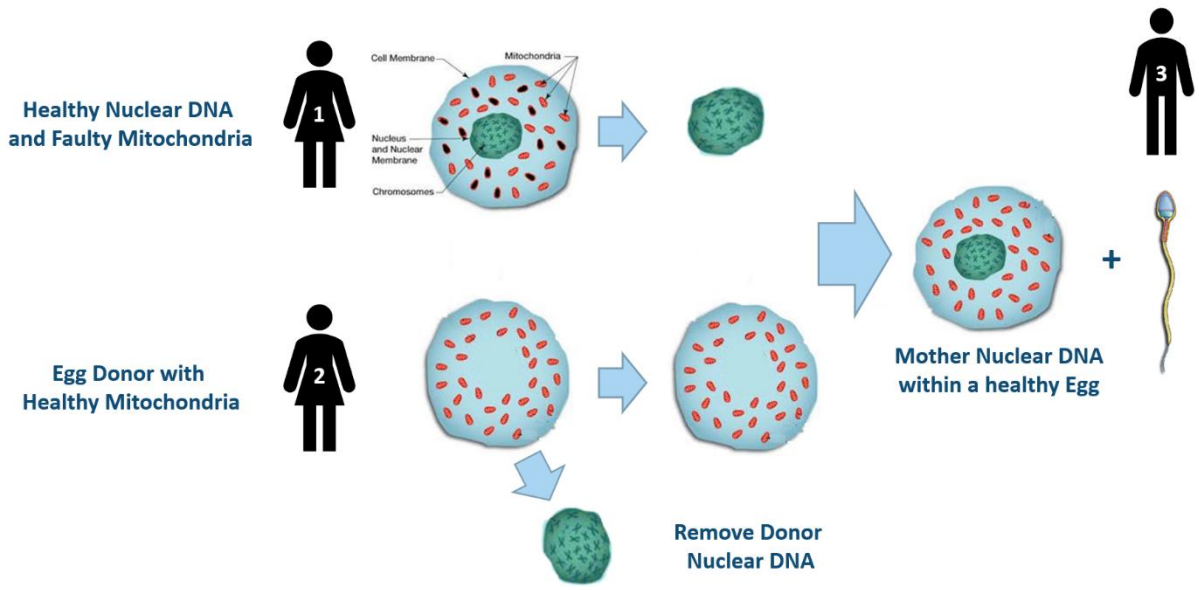

Fig. 1.4 | Mitochondrial Replacement Therapy. Mothers with known mitochondrial diseases are now able to give birth to children with no or low mtDNA mutation load through this approach which is based on in vitro fertilization and use of mitochondria from a healthy donor.

advances with MRT have opened an avenue for preventing the transfer of mitochondrial defects from mother to child (Fig 1.4).

In regards, to people who have already been born with mitochondrial diseases or have the acquired type of mitochondrial diseases, there has also been some advances. One interesting approach is that of the Boominathan's group, where allotropic expression of mitochondrial genes in the nucleus provides the nucleus with the genes that are otherwise made by the mitochondria. This in turn ensures that mitochondrially-encoded RNAs and proteins can be made even if there are defects in mtDNA. In 2016, the scientists successfully demonstrated that they can efficiently replace missing mitochondrial *ATP8* gene in cells from a human patient with an *ATP8* mutation, and restore cells ability to produce energy through oxidative phosphorylation, which is the most efficient pathway [15].

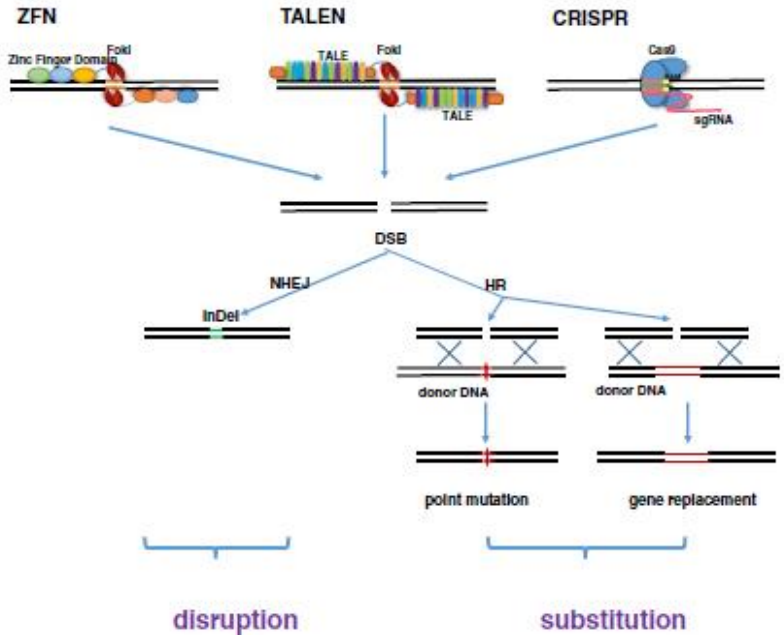

Fig. 1.5 | Genome Editing Strategies. Genome editing strategies which allow for DNA substitution or gene disruption are Zinc Finger Nuclease (**ZFN**), Transcription Activator-Like Effector Nuclease (**TALEN**), and Clustered Regularly Interspaced Short Palindromic Repeats/Cas9 nuclease (**CRISPR/Cas9 system**). Adapted from [4].

With advances in genome-editing strategies (Fig 1.5) such as Zinc Finger Nuclease (ZFN), Transcription Activator-Like Effector Nuclease (TALEN), and Clustered Regularly Interspaced Short Palindromic Repeats/Cas9 nuclease (CRISPR/Cas9 system), there have also been some attempts that use gene therapy approaches by substituting for the defective base pairs or disrupting the defective gene.

In 2018, Gammage et al. showed that they were able to use mitoZFN to produce large heteroplasmic shifts in phenotype and rescue patient-derived culture cells and in vivo mouse models with the point mutation m.5024C>T in mitochondrial $tRNA^{Ala}$ ($mt\text{-}tRNA^{Ala}$) [16].

Using mitoTALEN, Campbell and Ekker, manipulated mtDNA in vivo and in vitro for reverse genetics application, in 2018. They demonstrated that they were able to successfully delete ND4 gene, commonly found in LHON, in zebrafish embryos. Additionally, they demonstrated that they can successfully create large deletions in addition to smaller ones, by recreating a large deletion spanning ND5 to ATP8, which is commonly found in human diseases like Kearns-Sayre syndrome (KSS) and Pearson syndrome[17].

While the human-made ZFN and TALEN are more efficient gene editing strategies than CRISPR/Cas9 and have few off-target effects, they are time and labor intensive, in addition to being a cost-heavy approach and as such are not feasible strategies at this time. Thus, a more viable gene editing strategy would be the CRISPR/Cas9 system. However, while this genome editing strategy has been feasible in editing genomic DNA, it cannot be used for mitochondrial genome because (1) a prerequisite for CRISPR/Cas9 gene editing is to import nucleic acids to the site of editing, and CRISPR/Cas9 is unable to import nucleic acids to mitochondria, (2) there is not an efficient endogenous RNA import mechanism in mitochondria, and (3) there are not many approaches available for mtDNA manipulation [4].

Lastly, transplantation of mitochondria into the ischemic zone of myocardium has been shown to improve recovery in cardiac ischemia-reperfusion injury [18-28]. The mechanism of mitochondrial uptake is a question that is actively under investigation and some of the suggested mechanisms are actin-dependent endocytosis [18-28] and macropinocytosis [29]. This approach is similar in concept to our solution. Little is known about the intracellular fate of mitochondria during transplantation and in particular the bioenergetic consequences of mitochondrial transplantation. We addressed this question by studying how cellular bioenergetics are affected in short- and long-term after mitochondrial transplantation and the mitochondrial fate post-transplantation using mitochondrial genome sequencing.

1.5 OVERVIEW OF THE DISSERTATION

Mitochondrion, which is a membrane-enclosed micro-organelle, once deemed a free-living bacterium developed a symbiotic relationship with the ancestral eukaryotic cell through evolution. Inspired by this endosymbiotic origin of mitochondria I hypothesized and tested the feasibility of mitochondrial transplantation, which is discussed in Chapter 2. Mitochondria play a vital role in cellular bioenergetics and overall homeostasis; as such, their dysfunction leads to detrimental cellular consequences and clinical manifestations. While it has been recently shown that mitochondrial transplantation is feasible and may even alleviate the clinical manifestations of some critically-ill patients, not much is known about the intracellular consequences of mitochondrial transplantation and more specifically the bioenergetics consequences of mitochondrial transplantation, which is discussed in Chapter 3.

In this work, I have shown the feasibility of autologous, non-autologous, and interspecies mitochondrial transplantation using a variety of microscopy techniques. Furthermore, I have shown that bioenergetics consequences of mitochondrial transplantation in vitro using a metabolic flux analyzer. Currently, we are investigating whether the recipient cells adopt mitochondria for long-term through mitochondrial DNA sequencing studies (discussed in Chapter 4). Future directions of this work involve investigating the bioenergetics consequences of mitochondrial transplantation in cells with mitochondrial dysfunction.

Our motivation to pursue this line of research is to investigate the potential, safety, and efficacy of mitochondrial transplantation as a cellular biotherapy in hopes of eventually translating the findings from bench to bedside and mitigating diseases in which the mitochondria is deemed dysfunctional such as mitochondrial diseases, cardiovascular diseases, neurodegenerative diseases, and cancer.

CHAPTER 2: FEASIBILITY OF MITOCHONDRIAL TRANSPLANTATION

2.1 BACKGROUND

2.1.1. Confocal Microscopy. Confocal microscopy eliminates the blurred images otherwise caused by the fluorescence signals emitted by the fluorophores above and below the focal point. In confocal microscopy, a laser is used instead of the mercury lamp as the source of light, and images are taken with a digital camera with a pin hole that allows light of only one focal plane to be focused on the digital camera and all other light rays are blocked.

Laser scanning microscopy: In laser scanning microscope, a pinhole is used to block out the out of focus light, and an image is built pixel by pixel by collecting the emitted photons from the fluorophores.

Spinning disk microscopy: Rather than a single pinhole used in laser scanning microscopy, hundreds of pinholes are arranged in spirals on an opaque disk, which rotates at high speed.

2.1.2 Holotomography Microscopy. Holotomography microscopy uses the refractive index (RI) of a biological sample and provides a label-free quantitative imaging approach of microscopic phase objects.

2.1.3. Superresolution Microscopy. Superresolution Microscopy was conducted to overcome the limitation posed by the diffraction limit of the light and characterize the mitochondrial dynamics in higher resolution. In conventional light focused microscopy, the objective focuses the light to a point, but because light propagates as a wave it is not possible for the lens to focus all of the light into a single point and the light will be smeared, which gives to the diffraction limit of light (~200 nm) which is explained by $D = \frac{\lambda}{2NA}$. We acquired images on N-SIM and CSU-W1 SoRa instruments. N-SIM allows for superresoultion microscopy via combining structured illumination

microscopy with confocal microscopy, which provides twice the spatial resolution of conventional light microscopy (XY resolution of 120 nm). CSU-W1 SoRa allows for superresoultion microscopy via combining spinning disk confocal microscopy with optical pixel reassignment, which provides a 1.4x improvement beyond the optical limit (XY resolution of 120 nm).

2.2 METHODS

We performed microscopy studies as summarized in Fig. 2.1.

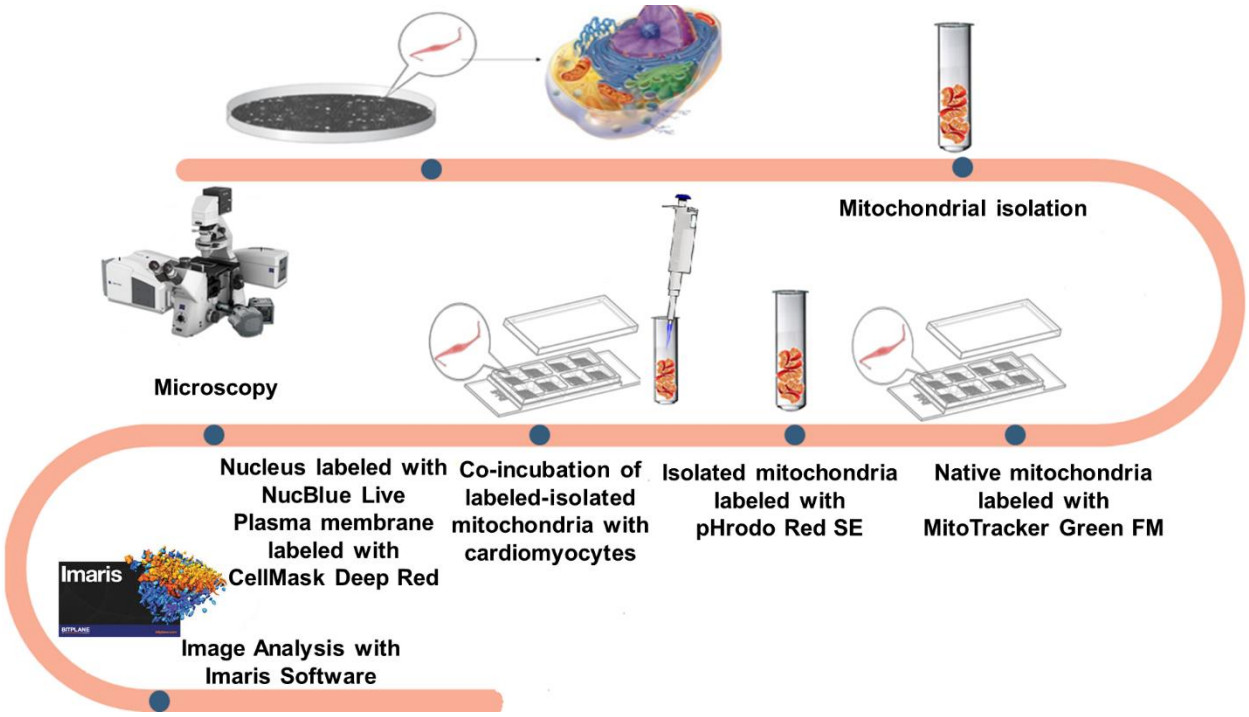

Fig. 2.1 | Schematic of our microscopy studies. Mitochondria were isolated using a commercially available isolation kit (ThermoFisher). The native mtiochondria were labeled with MitoTracker Green FM for 45 minutes at 37°C, isolated mitochondria were labeled with pHrodo Red SE for 30 minutes at 4°C, and the native mitochondria with MitoTracker Green FM (pre-co-incubation with the isolation mitochondria). The labeled-isolated mitochondria were transplanted to recipient cells (such as cardiomyocytes) via co-incubation. Nucleus and Plasma membrane were labeled before imaging, with NucBlue Live at room temperature for 20 minutes and CellMask Deep red for 10 minutes at 37°C. Microscopy data were analyzed with Imaris software and (Fiji image analysis software).

2.2.1 Cell Culture. Cells from the H9c2 cell line derived from rat embryonic hearts, L6 cell line derived from rat skeletal muscle cells, ARPE-19 cell line derived from human retinal pigmented epithelium, Jurkat cell line derived from peripheral blood of a patient with acute T cell leukemia (ATCC, Manassas, VA), and NHDF-Neo cell line derived from the dermis of human neonatal foreskin (Lonza, Basel, Switzerland) were grown per manufacturer's instructions. H9c2 and L6 cells were grown in complete growth medium, which consisted of Dulbecco's Medium (DMEM, high glucose, pyruvate), fetal bovine serum (FBS) to a final concentration of 10% and penicillin streptomycin (pen strep) to a final concentration of 1% (ThermoFisher Scientific, Waltham, MA).

ARPE-19 cells were grown in DMEM: F-12 Medium (ATCC), FBS to a final concentration of 10% and pen strep to a final concentration of 1% (ThermoFisher Scientific). ARPE-19 rho zero cells used in this work, were developed in Prof. Kenney's laboratory through long-term exposure of ARPE-19 cells to Ethidium Bromide. ARPE-19 rho zero cells were grown in the same media as ARPE-19 cells, with supplementation of 50 µg/mL of Uridine (SigmaAldrich). Jurkats (Immortalized T cells) were grown in RPMI-1640 Medium (ATCC), fetal bovine serum (FBS) to a final concentration of 10% and penicillin streptomycin (pen strep) to a final concentration of 1% (ThermoFisher Scientific). NHDF-Neo cells were grown in Dulbecco's Medium (DMEM, high glucose, pyruvate), fetal bovine serum (FBS) to a final concentration of 10%, Glutamax 2x to a final concentration of 2%, non-essential amino acids to a final concentration of 1%, and penicillin streptomycin (pen strep) to a final concentration of 1% (ThermoFisher Scientific). To conserve the myoblastic properties of H9c2 cells, the cells were grown at a seeding density of 1×10^4 viable$\frac{\text{cells}}{\text{cm}^2}$ and passaged when about 80% confluent (~every three days). Jurkats were maintained at a cell concentration between 1×10^5 and 1×10^6 viable$\frac{\text{cells}}{mL}$.

2.2.2 Mitochondrial Isolation. Mitochondria were isolated through differential centrifugation using a commercially available isolation kit following the reagent-based method detailed on the manufacturer's protocol (ThermoFisher Scientific). Purity of mitochondrial organelle isolate was prioritized over the yield. Accordingly, after nuclei and cell debris was fractionated and removed, to reduce lysosomal and peroxisomal contaminants, the samples were centrifuged at 3,000 rcf instead of 12,000 rcf to obtain the cytosol and mitochondria fractions, followed by wash and centrifugation of the mitochondrial fraction at 12,000 rcf. The mitochondrial pellet was kept on ice and followed immediately by transplantation.

2.2.3 Fluorescent Labeling. Native and transplanted mitochondria, nucleus, and plasma membrane were fluorescently-labeled for the microscopy studies as follows.

Native Mitochondria: Native mitochondria were labeled with MitoTracker Green FM with ex/em 490/516 nm (FITC channel for detection). MitoTracker Green FM dyes have a mildly thiol reactive chloromethyl moiety and localize to mitochondria regardless of mitochondrial membrane potential, through making specific interactions with the mitochondrial membrane proteins and/or lipids [30]. To make a stock solution of 1mM, 75 µL of DMSO was used to dissolve the lyophilized MitoTracker, and 2.5 µL of this was added to 4 mL warmed PBS (10x), pH 7.4 to make the working solution which was added to the cell culture plate at 37°C for 45 minutes to label the native mitochondria, followed by two washes with sterile PBS (ThermoFisher Scientific).

Transplanted Mitochondria: Isolated mitochondria were labeled with pHrodo Red Succinimidyl Ester (SE) with ex/em 560/585 nm (TRITC/m-cherry channel for detection). PHrodo Red SE produce stable carboxamide bonds with the amine groups on mitochondrial membrane proteins and/or lipids [31]. Once the pHrodo Red SE powder is dissolved in DMSO, it should be used immediately; thus, single-use aliquots were prepared. To do so the powder was dissolved in 1 mL of Methyl Cyanide/Acetonitrile (MeCN) and aliquoted into single use tubes (20 µL each), which was subsequently followed by evaporating off the MeCN to bring it back to powder. The aliquots were stored at -20C in sealed bags with desiccant packs. To label the isolated mitochondria, 20 µL of DMSO was added to each single-use aliquot, for a final concentration of 1 mg/mL. For mitochondria isolated from every 20 million cells, 20 µL of this working solution was used and incubated with the dye for 30 minutes at 4ºC, followed by centrifugation at 12,000 rcf for 5 minutes and wash with sterile PBS two times (ThermoFisher Scientific).

Nucleus: Cell nucleus was labeled with NucBlue Live reagent (Hoechst® 33342 dye) with ex/em 360/460 nm (DAPI channel for detection) which fluoresces when bound to DNA. One drop of reagent was used for every milliliter of media at room temperature and incubated for 15 minutes before imaging (ThermoFisher Scientific).

Plasma Membrane: Cell plasma membrane was labeled with CellMask Deep Red Plasma Membrane stain with ex/em 649/666 nm (Far red channel for detection). Unlike most plasma membrane stains which are typically lipophilic in nature, which offer a very narrow window for imaging, CellMask plasma membrane dye is amphipathic, which provides the lipophilic condition for membrane loading at the same time as providing a negatively charged hydrophilic environment for the dye to be anchored to the plasma membrane. Nevertheless, the dye eventually penetrates through the plasma membrane and gets inside the cells after ~30-90 minutes which is the reason why the dye is detected inside the cells in some of the images provided below. A fresh 1x working solution of the dye was prepared before use by adding 10 µL of the dye to 10 mL of PBS (10x), pH 7.4 solution and incubated with cells at 37°C for 10 minutes before imaging. The staining solution was removed by three sterile PBS washes (ThermoFisher Scientific).

2.2.4 Mitochondrial Transplantation. The isolated mitochondria were resuspended in PBS (10x), pH 7.4 solution, and mitochondria were transplanted into recipient cells via co-incubation on ice (4°C) for 30 minutes, in dark. For suspension cells such as Jurkats, before the 30 minutes co-incubation period, once the mitochondria were added to recipient cells the sample was centrifuged at 125 rcf for 5 mins. Mitochondria that were not internalized by the cell were removed from the media, by performing a wash step after 24-hour.

2.2.5 Microscopy. For imaging purposes, a day before mitochondrial isolation and transplantation, cells were plated at 50K on a µ-slide 8-well ibiTreat slide (ibidi, Martinsried, Germany) and at 100K on 35 mm dish (ibidi). Mitochondrial transplantation was visualized using widefield microscopy, confocal microscopy, holotomagraphy microscopy, and to overcome the limitation posed by the diffraction limit of the light, by superresolution microscopy. The respective data were analyzed using Fiji image analysis software and IMARIS software.

2.3 RESULTS

Inspired by the endosymbiosis theory of mitochondrial origin, we hypothesized and tested whether co-incubation of isolated mitochondria with cells would allow for mitochondria's uptake by the cell. First, we evaluated autologous mitochondrial transplantation of rat cardiomyocyte H9c2 cells.

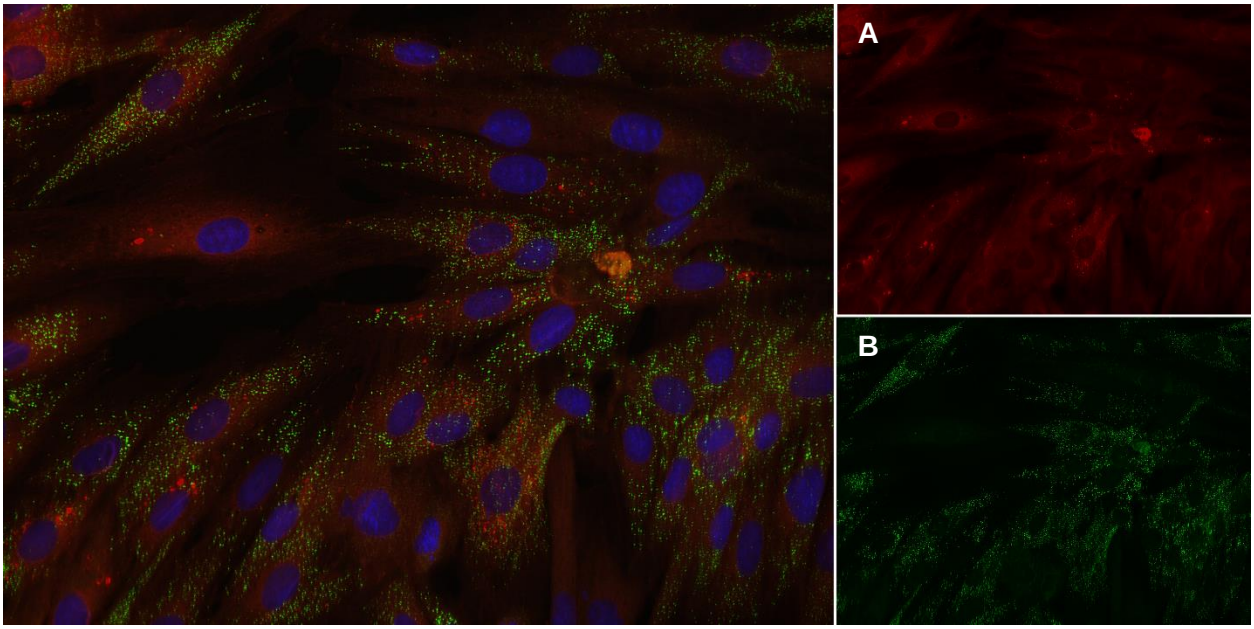

Fig. 2.2 | Feasibility of autologous mitochondrial transplantation. The newly internalized mitochondria (from H9c2 cardiomyocyte) labeled with pHrodo Red SE (A), the cell's native mitochondria labeled with MitoTracker Green FM (B), and the nucleus is labeled with NucBlue Live. The image was taken after the 28-hour time-lapse had been concluded. Images were acquired with Keyence structured illumination epifluorescence microscopy, 40x objective. NA: 0.95 [5].

Based on a 28-hour time-lapse study (Figs. 2.2 and 2.3), we observed mitochondrial internalization at various time points (with the shortest time being around 4 hours) and visualized the dynamics of mitochondrial internalization in time (Fig. 2.3). The cells remained viable for the duration of the experiment while the internalized mitochondria appeared to undergo fission and fusion dynamics based on the propagation of the pHrodo Red signal to the entire cell (Fig 2.3).

From a mechanistic perspective, in labeling the isolated mitochondria with pHrodo Red SE, the succinimidyl ester group interacts with the amine group on the mitochondria and forms a covalent amide bond. Nevertheless, to ensure the specificity of the detected signal representing mitochondrial internalization, we performed a set of control experiments with four groups as

described in Table 1. All four groups lacked isolated mitochondria. If pHrodo Red were to passively internalize into the cells, we would have expected to detect signal in the red channel for

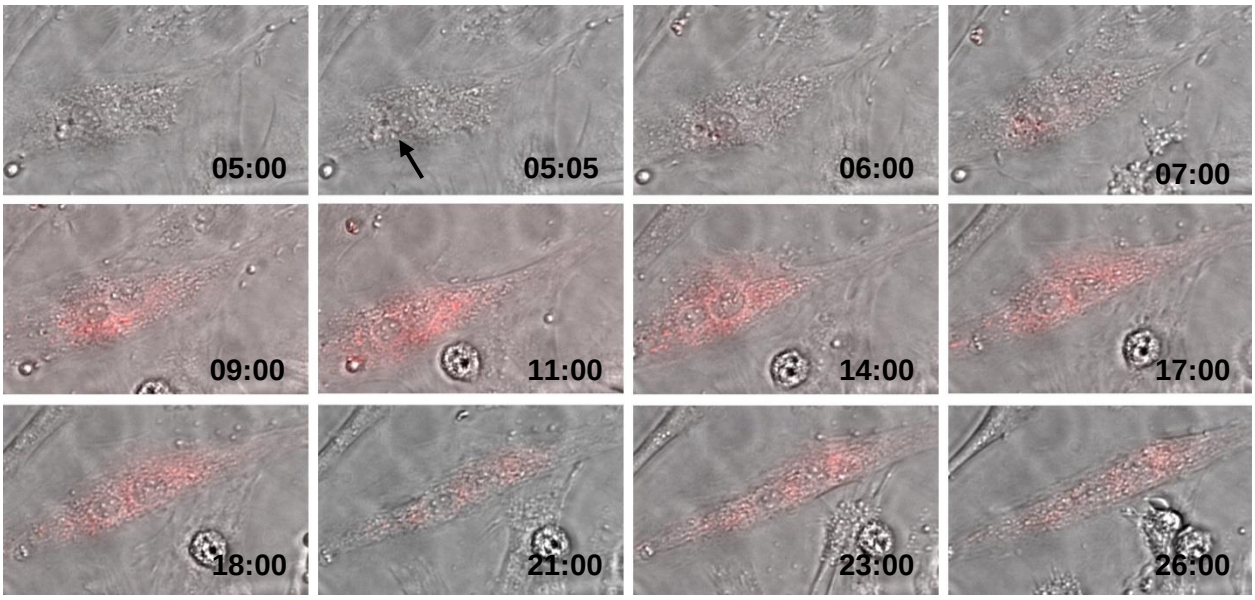

Fig. 2.3 | Dynamics of Mitochondrial Internalization. The isolated mitochondria labeled with pHrodo Red Succinimidyl Ester (SE) are being internalized into the rat H9c2 cardiomyocytes through co-incubation. Hour 5:00 represents the cardiomyocytes before mitochondrial internalization. The media contains the fluorescently-labeled mitochondria. Since pHrodo Red SE fluoresces brightly red only after the cell has internalized it, no florescence is yet observed. At 5:05, the cardiomyocyte starts taking in the mitochondria, as indicated by the red fluorescence signal (black arrow). As time passes, more mitochondria are internalized into the cell. Moreover, there are interactions between the mitochondria themselves, which are assumed to represent the dynamics of fusion and fission processes. Images were acquired with Olympus IX83, 20x objective, NA: 0.45 [5].

Table 1 | Mitochondrial Transplantation Validation Experiment

	Group Descriptions
1	pHrodo Red SE dye present in the media, with no cell plated
2	cells in the **absence** of pHrodo Red SE dye in the media.
3	cells in the **presence** of pHrodo Red SE dye in the media.
4	cells in the **presence** of pHrodo Red SE dye in the media, and native mitochondria fluorescently labeled with MitoTracker Green FM to control for proper function of microscope and fluorescent signal detection.

group 3 and 4. For group 4, the native mitochondria were labeled with MitoTracker Green FM to control for proper function of microscope and fluorescent signal detection. No fluorescence signal was detected in the red channel for any of the groups. Collectively, our experiments showed that the pHrodo dye by itself cannot passively internalize, and consequently the pHrodo-labeled autologous mitochondria actively internalize into the cells (Fig. 2.4).

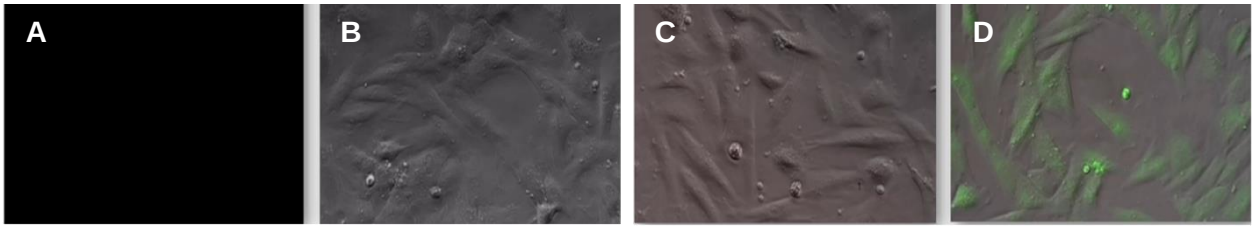

Fig. 2.4 | Validation of the active internalization of mitochondria. To investigate whether the pHrodo Red SE dye by itself can get passively internalized into the cell or not. **A.** pHrodo Red alone & no cells (Group1). **B.** cells only & no dye (Group 2). **C.** cells & pHrodo Red (Group 3). **D.** cells, native mitochondria labeled w/ MitoTracker Green FM & pHrodo Red (Group 4). All four groups lacked isolated mitochondria. There was no signal detected in the red channel, indicating that the pHrodo dye cannot get passively internalized into the cell. Images were acquired with Olympus IX83 , 20x objective, NA: 0.45.

We were interested to determine how the population of transplanted mitochondria compare to the native mitochondria and characterized the efficacy of mitochondrial transplantation using IMARIS software in 37 cells (Fig. 2.5). While in a few cells (four) there were as many transplanted

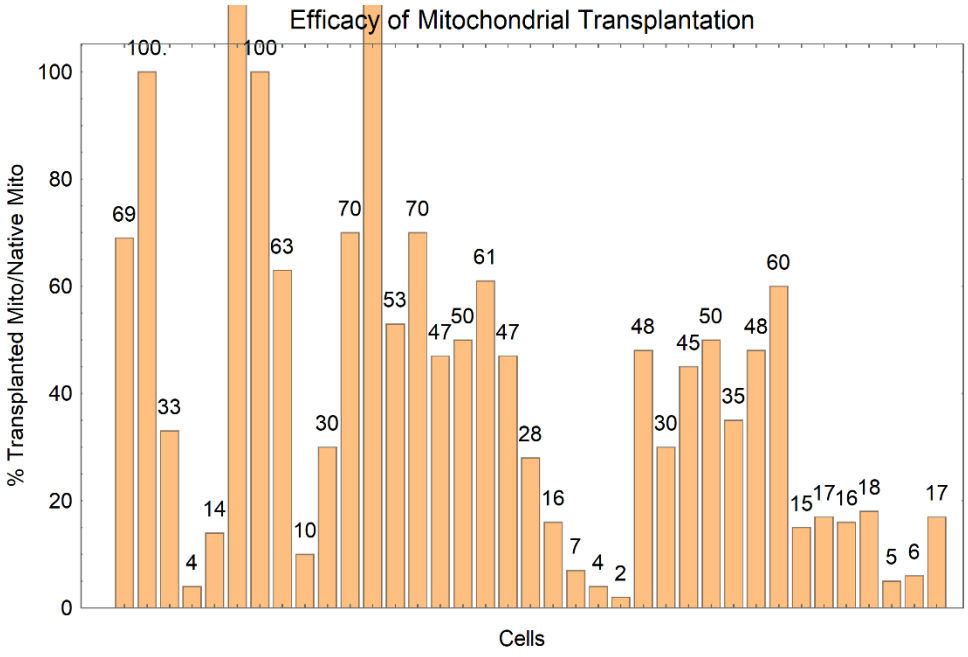

Fig. 2.5 | Efficacy of mitochondrial transplantation. Using IMARIS image analysis software the efficiency of mitochondrial transplantation was calculated. Overlapping cells were excluded from the analysis and only 37 cells with clear boundaries were used. The average percentage of transplanted mitochondria to native mitochondria was 66.1% with inclusion of 4 outlier cells (with very high ratio of transplanted to native mitochondria), and 32.9% without the inclusion of the outlier population.

mitochondria as the native mitochondria, if not more, for the majority of cells, the transplanted population were about 30-40% of the native mitochondria population.

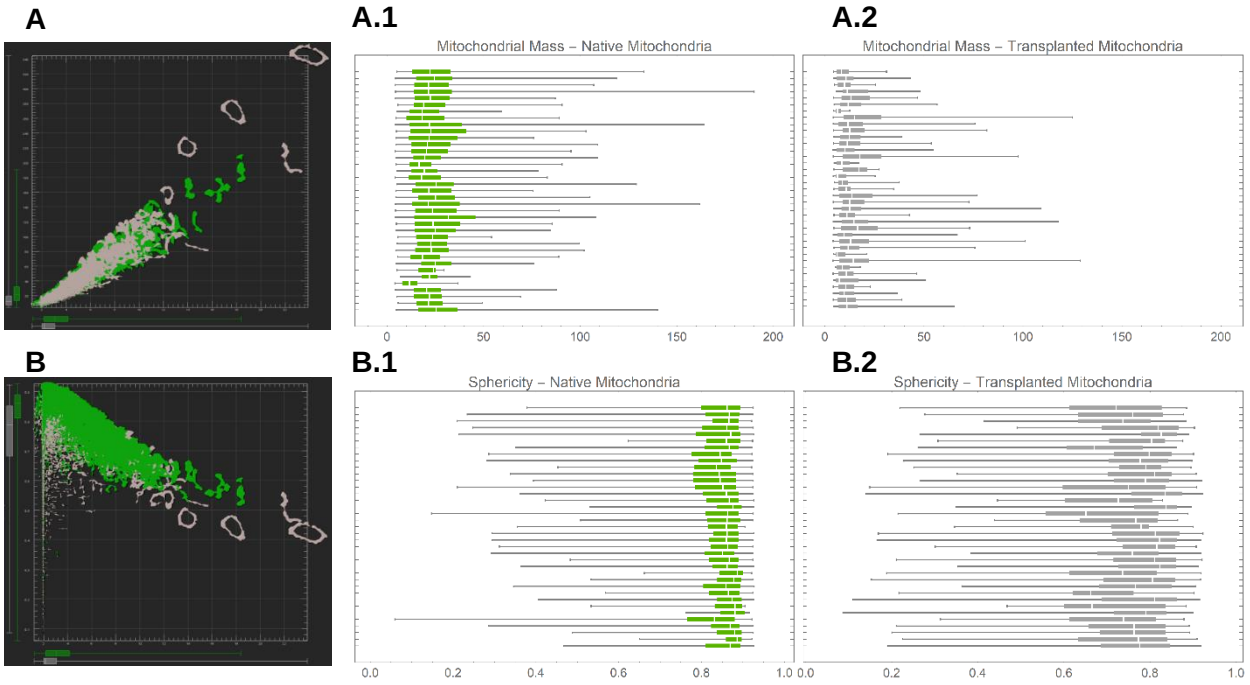

Fig. 2.6 | Mitochondrial mass and shape post mitochondrial transplantation. Using IMARIS image analysis software mitochondrial mass (A) and shape, evaluated by sphericity (B), were compared and contrasted between transplanted mitochondria and native mitochondria for a population of 47 cells with a total of 9804 native mitochondria and 4348 transplanted mitochondria. **Top.** Mitochondrial Mass. **Bottom.** Mitochondrial Shape (Sphericity). The Left panels shows the comparison for the aggregate results, with native mitochondria represented in green and transplanted mitochondria in gray. The right two panels, A.1 & A.2 and B.1 & B.2, represent the mitochondrial mass and sphericity values for native and transplanted mitochondria, respectively with native mitochondria represented in green and transplanted mitochondria in gray.

We discovered that not all cells uptake mitochondria similarly and some were more successful than others. We also compared and contrasted mitochondrial mass and shape (evaluated via sphericity) in transplanted and native mitochondria, using IMARIS software. (Fig. 2.6). Overall, mitochondrial mass and morphology appeared to be comparable in the transplanted population to that of the native mitochondrial population.

After successfully demonstrating the feasibility of autologous mitochondrial transplantation, we tested whether cells would similarly uptake non-autologous mitochondria (Fig. 2.7). Mitochondria isolated from rat L6 skeletal muscle cells were internalized by the rat cardiomyocyte H9c2 cells. This set of experiment showed that non-autologous mitochondrial transplantation is possible.

Next, we investigated interspecies mitochondrial transplantation by using isolated mitochondria

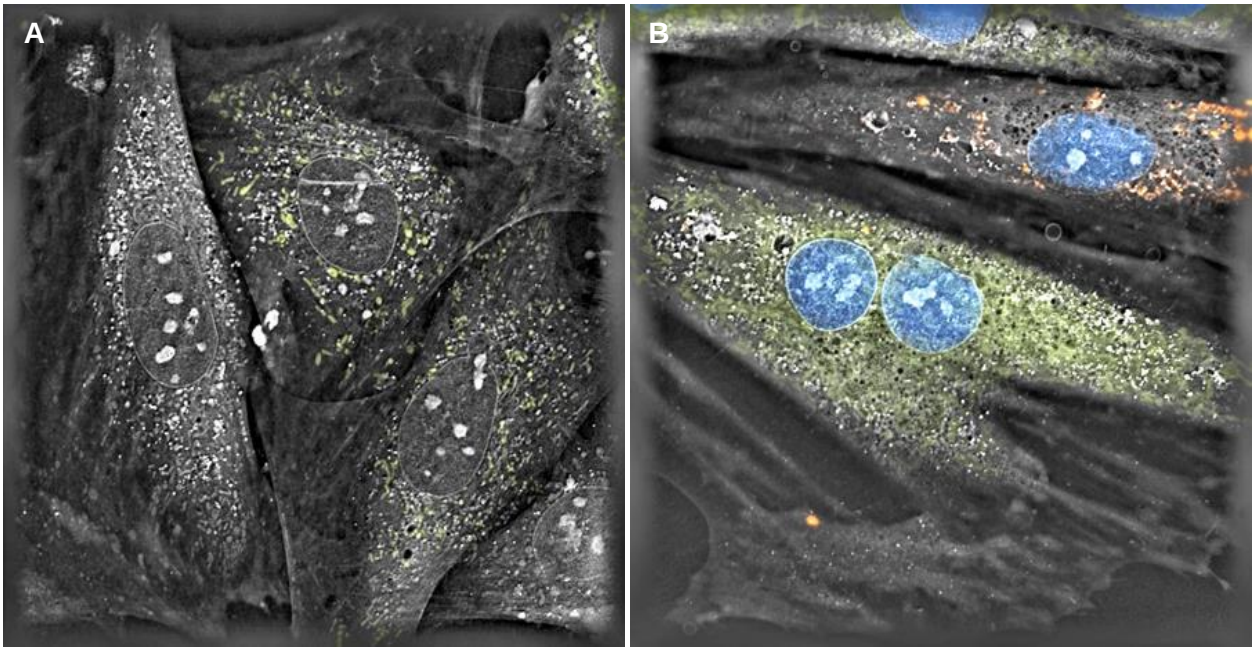

Fig. 2.7 | Feasibility of Non-autologous Transplantation. Mitochondria from rat L6 skeletal cells were transplanted into rat H9c2 cardiomyocytes. **A.** Transplanted mitochondria were labeled with MitoTracker green FM. **B.** Transplanted mitochondria were labeled with pHrodo Red SE, native mitochondria with MitoTracker Green FM, and nucleus with NucBlue Live. Images were acquired on Nanolive holotomography microscope, 100x objective, NA:1.4 [5].

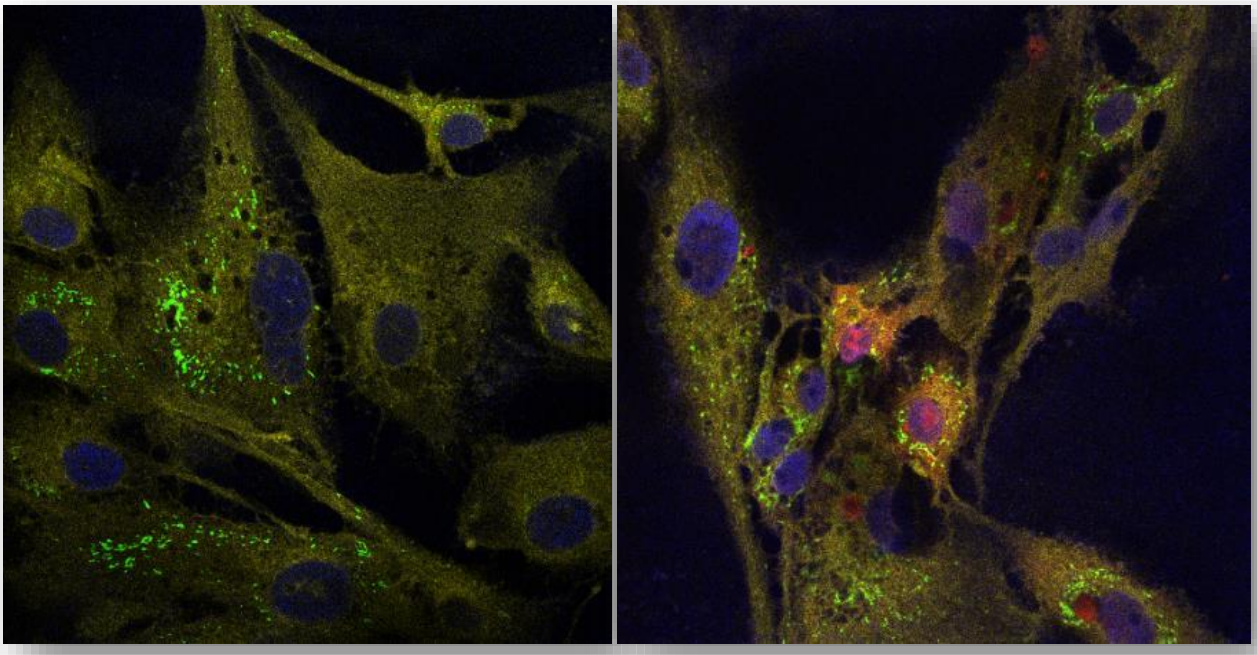

Fig. 2.8 | Feasibility of Interspecies Transplantation. Mitochondria from rat L6 skeletal cells, labeled with pHrodo Red SE was transplanted into human ARPE-19 retinal epithelial cells. Native mitochondria were labeled with MitoTracker Green FM, nucleus with NucBlue Live, and plasma membrane with Cellmask Deep Red Plasama Membrane. **A. Pre-transplant** and **B. Post-transplant**. Images were acquired with Zeiss Laser Scanning Confocal Microscope 780, 40x objective, NA: 0.75.

from the rat L6 cells and transplanting them into the human ARPE-19 retinal cells (Fig. 2.8). Similar to the previous experiments, mitochondria were successfully internalized into the cells and the feasibility of mitochondrial transplantation from rat to human cells was demonstrated.

Additionally, we transplanted mitochondria into rho zero mitochondrial-depleted cells (from ARPE-19) as described in Table 2, to study mitochondrial transplantation effects in cells with mitochondrial dysfunction (Fig. 2.9).

Table 2 | Mitochondrial Transplantation in Rho Zero Cells

	Group Descriptions
1	ARPE-19 WT cells
2	Post-transplant ARPE-19 Rho° cells, grown in media lacking uridine supplementation at the time of transplantation.
3	Post-transplant ARPE-19 Rho° cells, grown in media supplemented with uridine for the first 24-hour after transplantation and then changed to media lacking uridine supplement thereafter
4	ARPE-19 Rho° cells grown in media lacking uridine supplement

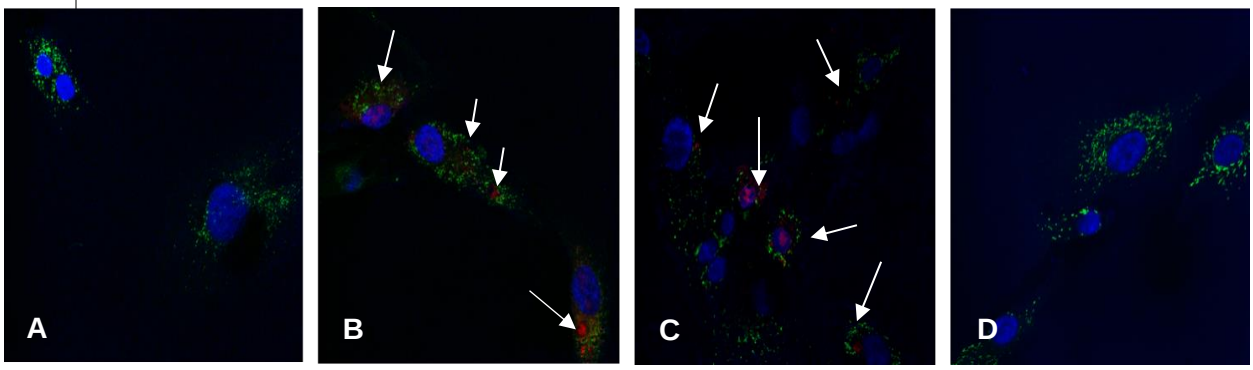

Fig. 2.9 | Mitochondrial transplantation in rho zero mitochondrial-depleted cells. Interspecies mitochondrial transplantation of rat L6 skeletal cells in human ARPE-19 retinal cells. **A.** ARP-19 WT cells. **B.** ARPE-19 rho zero cells post-mitochondrial transplantation in WT media. **C.** ARPE-19 rho zero cells post-transplantation initially in rho zero media with uridine supplement for 24-hour and moved to WT media for the second half of the 48-hour microscopy study. **D.** ARPE-19 Rho zero cells in medica lacking uridine supplementation. Transplanted mitochondria were labeled with pHrodo SE, native mitochondria with MitoTracker Green FM, and nucleus was labeled with NucBlue Live. Images were acquired with Zeiss Laser Scanning Confocal Microscope 780, 40x objective, NA:0.75.

We also successfully transplanted mitochondria into immune cells, specifically immortalized T cells (jurkat cells) as shown in Fig. 2.10. And lastly, we used superresolution microscopy to visualize mitochondria in higher resolution post-transplantation (Fig. 2.11).

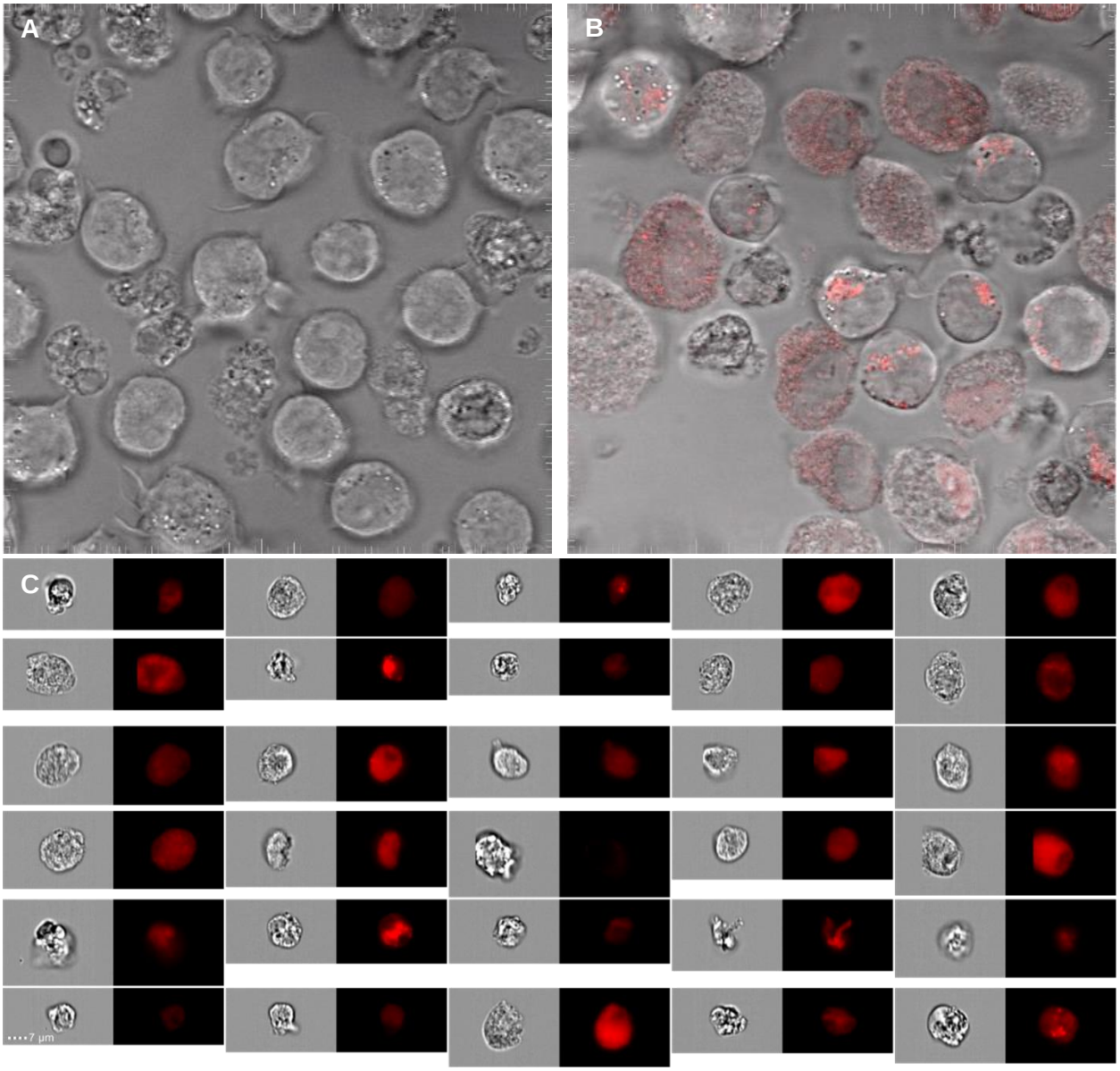

Fig. 2.10 | Mitochondrial Transplantation into T cells. Non-autologous mitochondria from human dermal fibroblast NHDF-Neocells were labeled with pHrodo SE and transplanted into Jurkats (Immortalized T cells). **A. Pre-transplant jurkats** and **B. Post-transplant jurkats.** pHrodo Red SE was excited by 561 nm laser and fluorescence detected for 561-642 nm range. Images were acquired on Zeiss Laser Scanning Confocal Microscope 780, 100x objective, NA:1.4. **C. Post-transplant jurkats visualized by flow cytometry.** pHrodo Red SE was excited by 488 nm laser and fluorescence was detected for channel 3 (560-595 nm). Images were acquired on Amnis ImageStream Flow Cytometer and analyzed with IDEAS (Image Data Exploration and Analysis Software), 60x objective, NA:0.9.

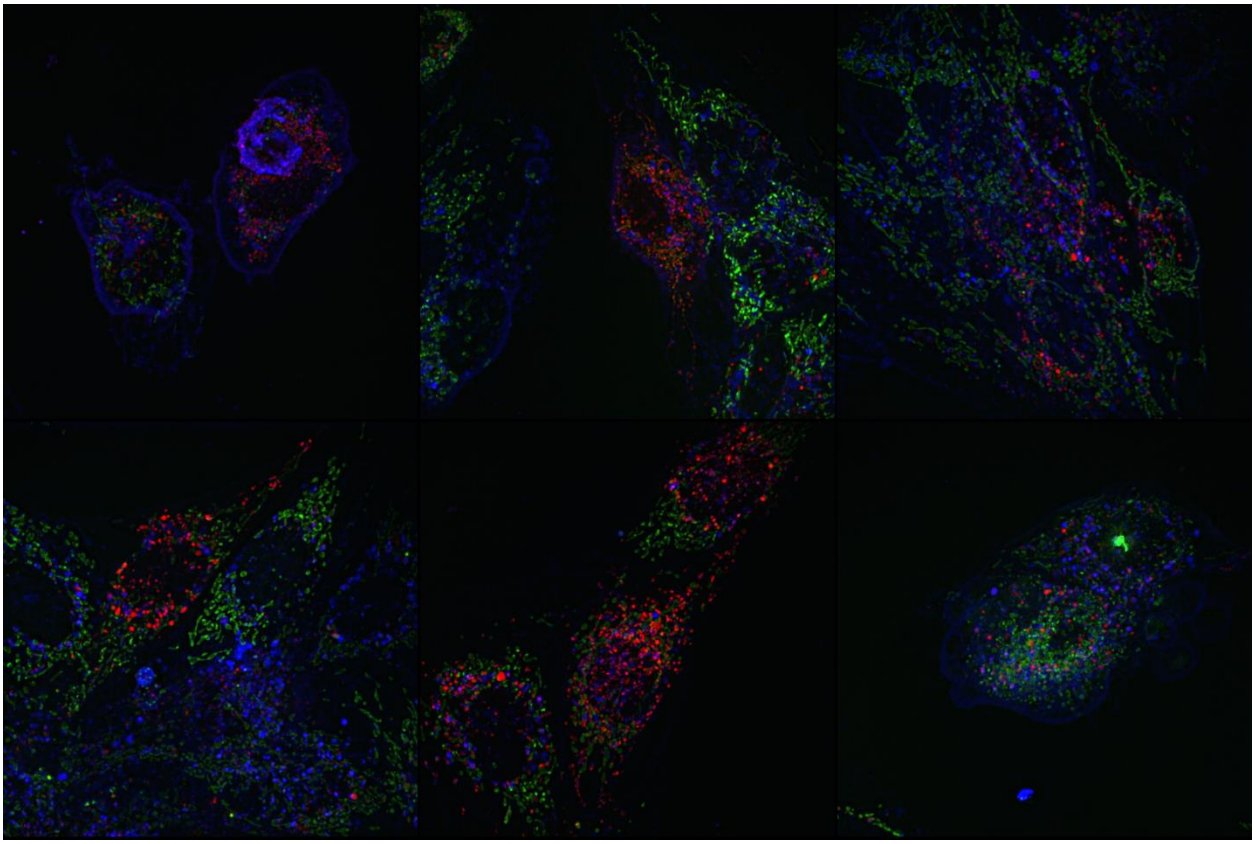

Fig. 2.11 | Superresolution microscopy of mitochondrial transplantation. Autologous mitochondria form L6 skeletal cells were used. Transplanted mitochondria were labeled with pHrodo Red SE and are depicted in red, native mitochondria were labeled with MitoTracker Green FM and are depicted in green, and the plasma membrane was labeled with CellMask Deep Red and is depicted in blue. Images were acquired on Nikon N-SIM, 100x objective, NA:1.4.

A 12-hour super resolution time-lapse microscopy was conducted on a Nikon Yokogawa CSU-W1SoRa instrument, to characterize mitochondrial morphology and dynamics between the transplanted mitochondria and native mitochondria. The images could not be analyzed due to the requirement of using IMARIS software, a subscription based software available on the computers at the Optical Biology Core, which became unavailable as a result of the UCI campus closure caused by the COVID-19 pandemic and hence the result could not be included in this dissertation.

2.4 DISCUSSION

We successfully demonstrated the feasibility of autologous (Fig. 2.2), non-autologous (Fig. 2.7) and interspecies (Fig. 2.8) mitochondrial transplantation. Moreover, we visualized the dynamics of mitochondrial internalization in time (Fig. 2.3). The cells remained viable for the duration of the 28-hour time-course study. The internalized mitochondria appeared to undergo fission and fusion dynamics based on the propagation of the pHrodo Red signal to the entire cell (Fig 2.3). The pHrodo Red SE label is sensitive to pH drop and fluoresces as endocytosed by the cell. The lack of fluorescence outside of the cell eliminates any doubt about the specificity of the detected signal. As shown in Fig 2.3, hour 5:00 represents the cardiomyocytes before mitochondrial internalization. The media contains the fluorescently-labeled mitochondria. Since pHrodo Red SE fluoresces brightly red only after the cell has internalized it, no florescence is yet observed. At 5:05, the cardiomyocyte starts taking in the mitochondria, as indicated by the red fluorescence signal (black arrow). As time passes, more mitochondria are internalized into the cell. The fluorescence intensity progressively decreases as the dye is segregated between the new daughter mitochondrion with each round of fission. Occasionally the fluorescence intensity increases locally, indicating new instances of mitochondrial internalization in those areas. With passing time, the pHrodo Red SE signal propagates through the entire cell, perhaps due to mitochondrial fission and fusion events between the transplanted and host mitochondria [5].

Based on our characterization of the efficacy of mitochondrial transplantation (Fig. 2.5), we discovered that not all cells uptake mitochondria similarly and some cells were more successful than others. A future direction of this work will be to develop a microfluidics platform that would allow mitochondrial transplantation in a more directed and controlled manner, where cells are feed into a channel one at a time, and co-incubated with mitochondria to increase the proportion of transplanted mitochondria with respect to native mitochondria and achieve a more uniform transplantation outcome.

We transplanted mitochondria into rho zero cells (from ARPE-19) as a model to study mitochondrial transplantation effects in cells with mitochondrial dysfunction (Fig. 2.9). Rho zero cells are mitochondrially-depleted cells that have small fragments of mt-DNA and as a result of mt-DNA mutation, do not have functional mitochondria. As, such they do not perform much oxidative phosphorylation and mostly rely on glycolysis. Furthermore, they are unable to synthesize uridine and need to be grown on media supplemented with uridine. Pyrimidine nucleoside uridine plays a critical role in maintaining cellular function and energy metabolism. Additionally, rho zero cells need pyruvate to oxidize excess cytoplasmic NADH via lactate dehydrogenase [32]. Hence, we hypothesized that rho cells would not able to grow on media lacking the uridine supplement, while post-transplant rho zero cells should have a better survival profile. Additionally, we included two environmental conditions for the transplant group, where the uridine supplementation was either removed at the time of transplantation or 24-hour after transplantation. This was to account for the time it takes the mitochondria to be internalized by the recipient cell and be incorporated by the cell. However, rho zero cells and both post-transplant rho zero groups similarly survived the media lacking uridine supplementation, with post-transplant rho zero cells only proliferating at a higher rate than rho zero cells. While the fluorescence microscopy images were taken 48-hour post-transplantation, we set up another experiment in which we investigated ARPE-19 rho zero survival in media lacking uridine. The cells remained alive up to 2-weeks, and could possibly survive even longer, as we did not follow the cells for a longer time, since they were able to grow in the media but at a slower rate. Based on this finding, rho zero bioenergetics (discussed in chapter 3), and the fact that the rho zero cells as a mitochondrial dysfunction model are artificially created in lab, we decided to use more representative models of mitochondrial dysfunction, mainly using cells from blood samples of patients with mitochondrial dysfunction and disorders. To this end, we tested and demonstrated

the feasibility of mitochondrial transplantation in immune cells and more specifically T cells by transplanting mitochondria from human NHDF-Neo fibroblasts into human jurkats (Fig. 2.10).

CHAPTER 3: BIOENERGETICS CONSEQUENCES OF MITOCHONDRIAL TRANSPLANTATION

3.1 BACKGROUND

To assess mitochondrial activity and function, oxygen consumption can be studied, as presence of oxygen is necessary to electron transport chain and ATP production. Thus, oxygen consumption rate (OCR), is representative of oxidative phosphorylation and reduced oxygen consumption may signal mitochondrial dysfunction, while increased oxygen consumption may mean improved mitochondrial function. Oxygen consumption can be measured through: (1) Clark oxygen electrode, (2) Fluorescence-based oxygen consumption, and (3) Metabolic Flux Analyzer.

In the Clark oxygen electrode, oxygen consumption is proportional to the current produced by the electrode. For this approach, an anode and cathode are in contact with an electrolyte solution covered by a semi-permeable membrane. Oxygen diffuses through the membrane to the cathode, where it is reduced. While the sensitivity of this method is good, its main disadvantage is that very low number of samples can be assessed at a time and it is not high throughput. Cells also need to be in suspension. On the other hand, the fluorescence-based oxygen consumption assay and use of metabolic flux analyzer provide a better throughput and are compatible with suspension and adherent cells. The fluorescent-based assay uses an oxygen-sensitive fluorescent probe and operates based on the ability of oxygen to quench the excited state of the probe. One such example is the potentiometric dye tetramethylrhodamine methyl ester (TMRM), which is readily sequestered by active mitochondria and fluoresces red-orange. Probe signal increases with oxygen consumption (oxygen concentration reduction) and the rate of signal increase is thus indicative of OCR. Use of a metabolic flux analyzer in bioenergetics analysis provides the most comprehensive assessment. In Seahorse Metabolic Flux Analyzer, the changes in both the pH and O_2 concentrations are detected in real-time by the solid-state sensor material that are spotted

on probe tips of the sensor cartridge. The changes in oxygen consumption (OCR) are used to determine the oxidative phosphorylation; and the changes in pH concentrations are used to determine the glycolytic activity, and an increase in conversion of pyruvate to lactate can be detected by an increase in extracellular acidification rate (ECAR).

Seahorse provides bulk measurement of the bioenergetics, and if single cell measurements are desired another (microscopy-based) method, called Fluorescence Lifetime Imaging (FLIM) can be conducted. As the name implies, in FLIM, the lifetime of a fluorophore, or in other words the time between the excitation and emission is found. FLIM (using the time domain) is another potential method to characterize the metabolic state and oxidative stress using phasor analysis of endogenous biomarkers. More specifically, absorbance measurements of free NADH and bound NADH are made for the control as a reference to mark the phasor lifetime on the plot. In its free state due to self-quenching the lifetime of NADH is about 0.4 ns which is significantly lower than that of the bound state, which is why FLIM can easily differentiate between free and protein bound forms of NADH. Two-photon laser microscope set to 740 nm is used to excite free and bound NADH, and the fluorescence emission can be collected using a Photomultiplier tube with a BP filter 420-500 nm. The raw intensity data is then transformed into polar coordinates by plotting sine and cosine. Similarly, oxidative stress can be assessed by determining long lifetime species (LLS) which in oxidative stress is characterized by clustering in the lifetime phasor plot. Through FLIM analysis using the phasor plot, the ratio of free to bound NADH is determined, the cell's mode of metabolism deduced, with bound NADH indicative of oxidative phosphorylation and free NADH indicative of glycolysis. Similarly, LSS population is assessed to evaluate stress prior and post mitochondrial transplantation.

In our studies, we used the Seahorse XF Flux Analyzer to assess bioenergetics, and since were interested in determining the changes in oxidative phosphorylation, Mito Stress Test Assay was performed. In the Mito Stress Test, after the basal measurement is recorded, the cells are sequentially treated with Oligmocyin, carbonylcyanide-p-trifluoromethoxyphenyl hydrazine (FCCP), and Rotenone + Antimycin A. Oligomycin is a phosphorylation inhibitor that by blocking ATP synthesis (Fig 3.1) allows users to deduce the oxygen consumption that was used for ATP production and proton leak in cells (Fig 3.2). FCCP is an uncoupler and serves as an electron transport chain accelerator that allows users to stimulate a situation of high energy demand/stress and determine the maximal respiration and spare respiratory capacity (Fig 3.2). And finally, Rotenone blocks complex I (Fig 3.1) and Antimycin A blocks complex III (Fig 3.1), which together block mitochondrial respiration, and allow users to determine the portion of oxygen that is consumed to meet non-mitochondrial respiration (Fig 3.2).

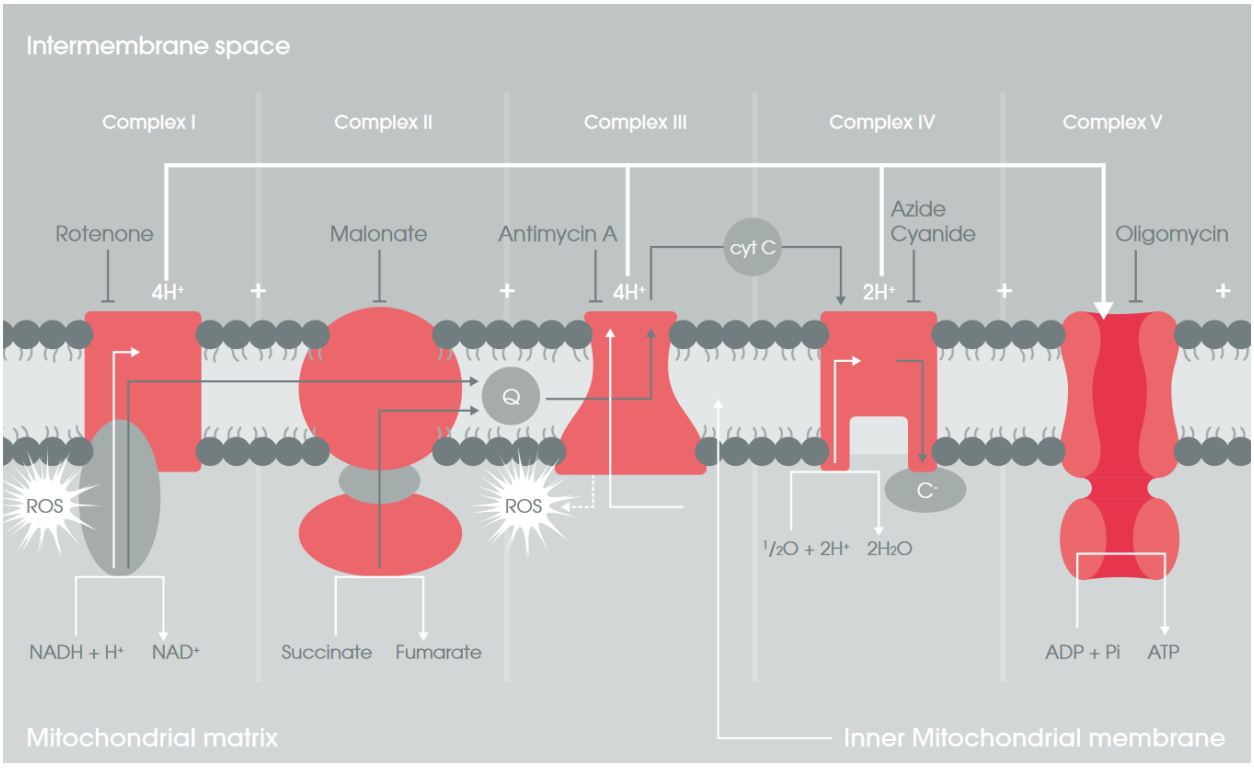

Fig. 3.1 | Oxidative Phosphorylation. Oxidative Phosphorylation, a major energy provider of the cell, consists of electron transport chain (complex I-IV), which creates a proton motive force that is used by ATP synthase (complex V) to synthesize ATP in a process called chemiosmosis. The inhibitors of complex I, II, III IV and V are: Rotenone, Malonate, Antimycin A, Azide Cyanide, and Oligomycin, respectively, and FCCP is an accelerator of ETC. Adapted from [1].

Basal respiration represents the amount of oxygen consumed by the cell to meet its energetic demands under baseline conditions and is determined using equation 1.

$$(1)\ Last\ Measurement\ before\ Oligomycin\ Injection - Nonmitochondrial\ Respiration\ Rate$$

ATP production represents the portion of basal respiration that was used by the cell to produce ATP by the mitochondria and is determined using equation 2.

$$(2)\ Last\ rate\ measurement\ before\ Oligomycin\ injection\ - Minimum\ rate\ measurement\ after\ Oligomycin\ injection$$

Proton leak is the remaining basal respiration not linked to ATP production, and can be a sign of damage, and is determined using equation 3.

$$(3)\ Minimum\ rate\ after\ Oligomycin\ injection - Non\ mitochondrial\ Respiration\ Rate$$

Coupling efficiency is an index that determines how efficiently the cell translates the proton motive force from the electron transport chain to ATP production, using equation 4.

$$(4)\ \frac{ATP\ Production\ Rate}{Basal\ Respiration\ Rate}\ x\ 100$$

Maximal respiration is the maximal oxygen consumed by the cell when the respiratory chain operates at maximum capacity, which causes rapid oxidation of substrates (sugars, fats, and amino acids) to meet the metabolic demands, and shows the maximum rate the cells can achieve, determined using equation 5.

$$(5) Maximum\ rate\ measurement\ after\ FCCP\ injection - Nonmitochondrial\ Respiration\ Rate$$

Spare respiratory capacity is an index that measures the cell's capability in responding to a situation of high energy demand/ stress, which allows to determine how closely the cell is respiring to its theoretical maximum and the cell's fitness or flexibility using equation 6.

$$(6)\ Maximal\ Respiration - Basal\ Respiration$$

And finally, non-mitochondrial respiration which represents the oxygen consumption that persists even in the absence of mitochondrial respiration due to a subset of cellular enzymes is determined using equation 7.

$$(7)\ Minimum\ rate\ measurement\ after\ Rotenone - Antimycin\ A\ injections$$

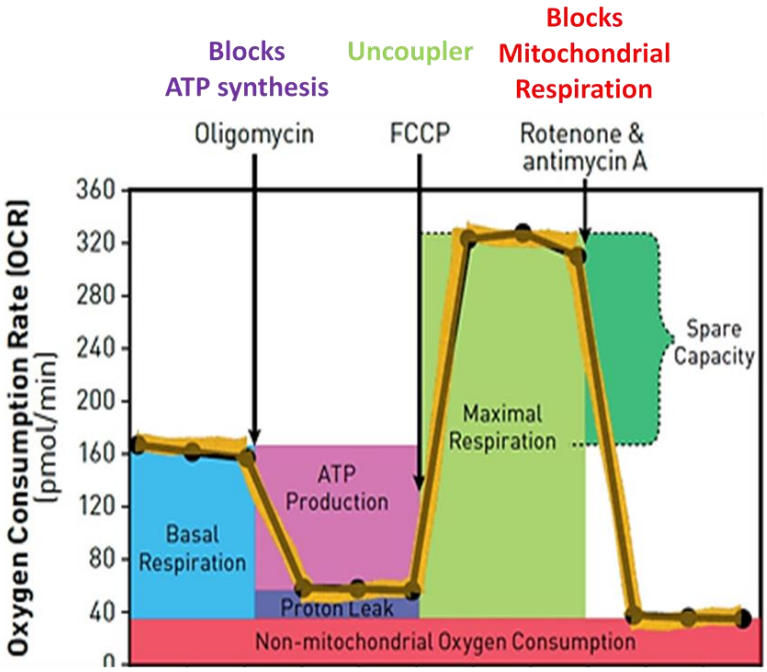

Fig. 3.2 | Mito Stress Profile. Bioenergetics parameters such as basal respiration, ATP production, proton leak, maximal respiration, spare respiratory capacity and non-mitochondrial oxygen consumption can be calculated using Mito Stress Test based on the oxygen consumption rate (OCR) in response to sequential treatment with Oligomycin, FCCP, and Rotenone & Antimycin. Oligomycin which is a phosphorylation inhibitor blocks ATP synthesis which allows to deduce the ATP production and proton leak in cells. FCCP which is an uncoupler serves as an electron transport chain accelerator and simulates a situation of high energy demand/stress. In doing so, maximal respiration is determined, which when used in conjunction with basal respiration reveals the cells' spare respiratory capacity. Rotenone blocks complex I and antimycin A blocks complex III, which when used together block mitochondrial respiration altogether and reveal the cells' non-mitochondrial oxygen consumption. Adapted from [6] .

3.2 METHODS

To investigate the bioenergetics consequences of mitochondrial transplantation, oxygen consumption rate (OCR) and extracellular acidification (ECAR) rates were measured post transplantation using a Seahorse XF24 Flux Analyzer (Agilent Technologies, Santa Clara, CA).

To determine whether oxidative phosphorylation can be restored to rho zero cells through mitochondrial transplantation, mitochondria from L6 skeletal cells (p.9) were isolated using a commercially available isolation kit (ThermoFisher Scientific) and mitochondria from 5 Million cells (100 mitochondria:1 recipient cell) were transplanted into ARPE-19 rho zero cells via co-incubation for 24 hours. After that any mitochondria not internalized into cardiomyocytes were removed by changing the culture media. ARPE-19 cells (rho zero and WT) were plated at cell seeding density of 50K, 72-hour before the Mito Stress Assay, since mitochondrial transplantation

Table 3 | Description of Groups for Bioenergetics Studies Post Mitochondrial Transplantation in Rho Zero Cells

	Group Descriptions
1	ARPE-19 WT cells
2	Post-transplant ARPE-19 Rho° cells, grown in media lacking uridine supplementation at the time of transplantation (WT media)
3	Post-transplant ARPE-19 Rho° cells, grown in media supplemented with uridine for the first 24-hour after transplantation and then changed to media lacking uridine supplement thereafter (Rho° media → WT media)
4	ARPE-19 Rho° cells grown in media lacking uridine supplement (WT media)
5	ARPE-19 Rho° cells grown in media supplemented with uridine supplement (Rho° media)

was directly done on the Seahorse Microplate (Agilent). The five groups included in this study are described in Table 3. Mito Stress Test was performed 48-hour post-transplantation.

To determine the bioenergetics consequences of mitochondrial transplantation in normal cells, mitochondria from L6 skeletal cells (p.9) were isolated (100 mitochondria: 1 recipient cell) using a commercially available isolation kit and transplanted into H9c2 cardiomyocyte cells (p.10). Isolated mitochondria were co-incubated with H9c2 cells for 24 hours. After that any mitochondria not internalized into cardiomyocytes were removed by changing the culture media. The transplantation experiments were done on regular tissue culture flasks (12-well and 96-well plates) and not the Seahorse Microplate. They day before mitochondrial transplantation, 320M cells were plated on a 12-well plate and 125K cells were plated on a 96-well, and mitochondria from 32 Million cells and 12.5 Million cells were transplanted to each plate, respectively. The day before running the Seahorse Mito Stress Assay, 40K cells were plated onto a Seahorse

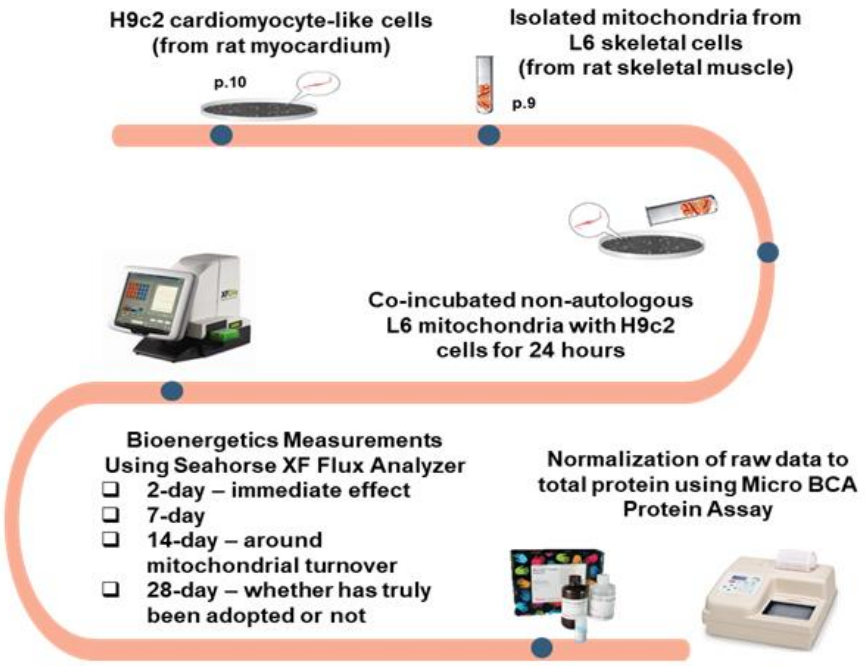

Fig. 3.3 | Schematic of our bioenergetics studies. Non-autologous mitochondria from L6 cells were used for transplantation into H9c2 cells via co-incubation. Bioenergetics measurements were conducted using a Seahorse metabolic flux analyzer post (a) 2-day (immediate effect), (b) 7-day, (c) 14-day (around mitochondrial turnover), (d) 28-day (after mitochondrial turnover, for true adoption) and raw data were normalized to total protein using Micro BCA Protein Assay.

microchamber plate. Bioenergetics studies for post mitochondrial transplantation in H9c2 is summarized in Fig. 3.3.

Bioenergetics measurements were performed, after sequential treatment with Oligomycin, FCCP, and Rotenone + Antimycin A (Agilent Technologies) post-transplantation and compared to that of the control group to investigate the effect of mitochondrial transplantation. For the studies of bioenergetics consequences of mitochondrial transplantation in ARPE-19 rho zero cells, a total of 8 post-transplant rho zero cells, 8 rho zero cells, and 4 WT cells were assessed. For Bioenergetics consequences of non-autologous mitochondrial transplantation in H9c2 cells, two sets of independent studies were done, with a total of 28 observation for the experimental group and 12 for the control group. Raw data were normalized to total protein concentration and data was analyzed on Wave Software (Agilent).

3.2.1. Seeding Cells in Agilent Seahorse XF24 Cell Culture Microplate. For ARPE-19 cells, since the transplantation experiments were performed directly on the Seahorse Microplate (Agilent Technologies), ARPE-19 cells were seeded at the optimized seeding density of 50K, 72-hour prior to the Mito Stress Assay. For the H9c2 cells, the transplantation experiments were performed on regular tissue culture flasks (12-well and 96-well plates). As such, post-transplant and control cells were seeded on the Seahorse Microplate, at the optimized seeding density of 40K, a day prior to the Mito Stress Assay. Cells were collected and resuspended in 100 µL of growth media and seeded at the optimized seeding density in each well with the exception of the background wells. For the background correction wells A1, B4, C3, and D6 only media was added. The plate was rested at room temperature in the tissue culture hood, with the lights turned off, for one hour to promote even cell distribution and reduce edge effects [33]. The plate was then moved to incubator for 5 hours to allow the cells to adhere to the plate, after which an additional 150 µL of growth media was added to the cells and returned to incubator to grow overnight. To ensure a

homogenous cell layer at the time of cell seeding and to not disturb the cells at the time of supplying the media, the pipette tip was held at an angle about halfway down to the side of the wells. The seeding surface of each well is 0.275 cm^2.

3.2.2. Hydration of Agilent Seahorse XF24 Sensor Cartridge. It is important to hydrate the sensor cartridge (Agilent) a day prior to running an XF assay (with the minimum hydration time of 4-hour). To hydrate the cartridge, the sensor cartridge was place upside down (to not damage the sensor probes) and 1 mL of XF Calibrant (Agilent) was added to each well of the utility plate, followed by placing the sensor cartridge onto the utility plate, submerging the sensors in the calibrant solution. Lastly, the sensor cartridge and utility plate were transferred to a non-CO_2 incubator, operating at 37 °C and humidified.

3.2.3. Washing Adherent Cells in Agilent Seahorse XF24 Cell Culture Microplate. On the day of performing the Mito Stress Test, the growth media must be washed and replaced with the assay media (which lacks bicarbonate buffer system and has low/no phenol red that would otherwise interfere with the measurements readings of the fluorescent probes). The assay media was prepared on the day of the assay, warmed to 37 °C with pH set to ~7.2-7.4 using a pH meter. To wash the cells, all but 50 µL (a volume that makes a crescent shape when the plate is tilted to the side) of the culture media was removed from each well, so that the cells are not disturbed. The cells were then rinsed with 1 mL of assay medium twice, leaving behind 50 µL each time, followed by addition of 450 µL of the assay medium. The microplate was then placed in a 37 °C incubator for 45 minutes prior to running the assay on the XF Flux Analyzer instrument.

3.2.4. Mito Stress Test Protocol. On the day of Mito Stress Test assay, the cells were washed as described above, and the instrument protocol was set up on the seahorse flux analyzer. Drug treatments (Oligomycin, FCCP, Rotenone + Antimycin A) were injected to the sensor cartridge ports, and the sensor cartridge and utility plate were inserted into the instrument. Once the

calibration was done, the utility plate was removed, and the microplate was loaded to run the assay.

3.2.5. Mito Stress Assay Specifications for ARPE 19 Cell.

Seeding Density Optimization: Based on previous experiments by the Mitochondrial Research Laboratory under supervision of Prof. Kenney, in which ARPE-19 cells were seeded at 10K, 20K, 30K, 40K, 60K, and 80K, the optimized cell seeding density for ARPE-19 was determined to be 50K.

FCCP Optimization: Based on previous experiments by the Mitochondrial Research Laboratory, the optimized final concentration for FCCP injection was determined to be 1µM of FCCP.

Assay Media: The Seahorse assays were performed in a Seahorse XF DMEM medium supplemented with glucose to a final concentration of 17.5 mM, sodium pyruvate to 1 mM, and L-glutamine to 2mM. The assay media were prepared on the day of Mito Stress Test assay and the pH was assed and set to ~7.2-7.4 using a pH meter.

Injections: Treatments were done sequentially in time, with final concentration of 1µM (0.91 µM to be exact) of Oligomycin injection into Port A, 1µM (0.91 µM to be exact) of FCCP injection into Port B, and 1µM (0.90 µM to be exact) of Rotenone + Antimycin A injection into Port C as detailed below:

- 12 µL of 2.5 mM Oligomycin was added to 3 mL XF assay media (injection concentration of 10 µM) and 50 µL of this solution was injected to Port A.
- 12 µL of 2.5 mM FCCP was added to 3 mL XF assay media (injection concentration of 10 µM) and 55 µL of this solution was injected to Port A.

- 12 µL of 2.5 mM Rotenone and 12 µL of 2.5 mM Antimycin A were added to 3 mL XF assay media (injection concentration of 10 µM) and 60 µL of this solution was injected to Port A.

Instrument Protocol: The instrument protocol used for ARPE-19 cells is as follows:

Calibrate
Equilibrate
Basal: 3 cycles, duration: 30 minutes
-3 minute Mix, 2 minute Wait, 5 minute Measure
Inject Port A (Oligomycin): 3 cycles, duration: 30 minutes
-3 minute Mix, 2 minute Wait, 5 minute Measure
Inject Port B (FCCP): 3 cycles, duration: 30 minutes
-3 minute Mix, 2 minute Wait, 5 minute Measure
Inject Port C (Rotenone + Antimycin A): 3 cycles, duration: 30 minutes
-3 minute Mix, 2 minute Wait, 5 minute Measure

3.2.6. Mito Stress Assay Specifications for H9c2 Cell:

Seeding Density Optimization: I plated H9c2 cells at seeding densities of 10K, 20K, 40K, and 80K to find the optimized cell seeding density which was experimentally determined to be 40K.

FCCP Optimization: Following the seeding density optimization, I used FCCP concentrations of 0.25 µM, 0.5 µM, 1.0 µM, and 2.0 µM for the optimized seeding density of 40K and the optimized FCCP concentration was found to be 1.0 µM.

Assay Media: The Seahorse assays were performed in a Seahorse XF DMEM medium supplemented with glucose to a final concentration of 10 mM, sodium pyruvate to 1 mM, and L-glutamine to 2mM. The assay media were prepared on the day of Mito Stress Test assay, by combining 97.0 mL of Seahorse XF DMEM Medium, pH 7.4, 1.0 mL of 1.0 M Glucose solution,

1.0 mL of 100mM Pyruvate solution, and 1.0 mL of 200 mM L-Glutamine solution and the pH was assed and set to ~7.2-7.4 using a pH meter.

Injections: Treatments were done sequentially in time, with final concentration of 1µM of Oligomycin injection into Port A, 1µM of FCCP injection into Port B, and 0.5 µM of Rotenone + Antimycin A injection into Port C as detailed below:

- 12 µL of 2.5 mM Oligomycin was added to 3 mL XF assay media (injection concentration of 10 µM) and 56 µL of this solution was injected to Port A.
- 12 µL of 2.5 mM FCCP was added to 3 mL XF assay media (injection concentration of 10 µM) and 62 µL of this solution was injected to Port A.
- 12 µL of 2.5 mM Rotenone and 12 µL of 2.5 mM Antimycin A were added to 3 mL XF assay media (injection concentration of 5 µM) and 69 µL of this solution was injected to Port A.

Instrument Protocol: The instrument protocol used for H9c2 cells is as follows:

Calibrate
Equilibrate
Basal: 3 cycles, duration: 24 minutes
    -3 minute Mix, 2 minute Wait, 3 minute Measure
Inject Port A (Oligomycin): 3 cycles, duration: 24 minutes
    -3 minute Mix, 2 minute Wait, 3 minute Measure
Inject Port B (FCCP): 3 cycles, duration: 24 minutes
    -3 minute Mix, 2 minute Wait, 3 minute Measure
Inject Port C (Rotenone + Antimycin A): 3 cycles, duration: 24 minutes
    -3 minute Mix, 2 minute Wait, 3 minute Measure

3.2.7. Total Protein Isolation and Quantification. Total protein was isolated using RIPA buffer (Thermofisher Scientific) and quantified using Bradford Assay (Thermofisher Scientific) for the ARPE-19 cells, and Micro BCA Assay (Thermofisher Scientific) for the H9c2 cells.

Raw data from Seahorse were normalized to total protein via the normalize tab on Wave software (Scale Factor of 10 should be used). Standard curve was created in both assays using values from absorbance measurements of known concentration of BSA solutions (ThermoFisher Scientific).

3.2.8. Quantitation of Mitochondrial Superoxide Production. To assess the production of superoxide by mitochondria, MitoSOX Red Mitochondrial Superoxide Indicator (ThermoFisher Scientific) was used. The day before running the MitoSOX superoxide production assay, 40K cells were plated onto a 96-well plate. At 2-day post-transplantation the cells were incubated with MitoSOX Red (5 μM) at 37 ºC for 10 minutes. The cells were then washed three times with sterile PBS. Using a fluorescence plate reader, MitoSOX Red was excited at 485 nm and fluorescence emission was measured at 590 nm. Fluorescence values were recorded for two groups of independent transplantation experiments and compared to a control group, with 10 observations for each group (Fig. 3.7).

3.2.9. Statistical Analyses. An unpaired two-tailed unequal variance t-test (Welch's Test) was used for the mean values of Seahorse bioenergetics data in Microsoft Excel. A Welch's Test, which is a more stringent test than the student t-test was used. This was done to account for the possibility of mitochondrial transplantation changing the bioenergetics both positively and negatively (two-tailed), possible different distributions of the control and transplant groups (unequal variance), and that the measurements were taken independently (unpaired). To check for normality, qq plots of the data were generated in R. The distribution in transplant appears in fact to be different from the control group. Most observations fell within the 95% confidence

interval, and overall the data were reasonably normally distributed. Results with $p < 0.05$ were considered as statistically significant. No statistical methods were used to predetermine the sample size. Sample size was based on experimental feasibility for proof of concept. The graphs presented in Figs. 3.5 - 3.8 were generated in Mathematica (Wolfram Research, Champaign, IL). Data from bar graphs presented in Figs. 3.5, 3.6, and 3.8 are means ± SEM and data from kinetic profiles in Figs. 3.5 and 3.6 are mean ± SD from n=2 independent experiments each with 14 biological replicates for the experimental transplant group and 6 biological replicates for the control group. For the 28-day post-transplantation experiment, 27 observations were recorded versus the 28 for all the other time-points, due to measurement failure in one of the wells.

A Welch's test was used to compare post-transplant cardiomyocytes' mean superoxide production to that of the control at the 5% level. Fluorescence values after MitoSOX-treatment were recorded from n=2 independent transplant groups and compared to n=1 control group, each with 10 biological replicates. No statistical methods were used to predetermine sample size. The fluorescence values are displayed as Box and Whisker plots in Fig. 3.8. The fluorescence measurement from the MitoSOX-treated control and transplant groups were normalized to the mean fluorescence measurement value of the untreated control. Mitochondrial superoxide production was reported as the normalized fluorescence values ± SD and presented as bar graphs in Fig. 3.8.

3.3 RESULTS

After we successfully demonstrated the feasibility of mitochondrial transplantation, we investigated the bioenergetic consequences of mitochondrial transplantation.

First, we hypothesized and tested whether mitochondrial transplantation in rho zero cells improves their bioenergetics, mainly restore oxidative phosphorylation (Fig. 3.4). The overall kinetics of oxygen consumption rate (OCR), representative of oxidative phosphorylation, increased in post-transplant rho zero cells vs. control rho zero cells, while the extracellular acidification rate (ECAR), representative of glycolysis, remained relatively the same. While the OCR kinetics increased, the changes in bioenergetics parameters in post-transplant rho zero cells were not statistically significant ($p > 0.05$) and the overall OCR profile resembled that of the rho zero cells and not that of the wild type ARPE-19 (Fig. 3.4).

Next, we hypothesized and tested whether the internalization of the transplanted non-autologous mitochondria leads to enhanced bioenergetics, by conducting Cell Mito Stress Test using a Seahorse XF24 Flux Analyzer. We measured the oxygen consumption rate (OCR), which represent the rates of oxidative phosphorylation and extracellular acidification rate (ECAR), which denotes the summation of acid (H^+) produced from glycolysis *and* the TCA cycle (via CO_2), when obtained through Mito Stress Test. Subsequently, we compared the results to the control groups with no transplantation event. Baseline and post-transplant rates were measured at four different time points: post 2-day to measure acute effects (Fig. 3.5), post 7-day, post 14-day to check bioenergetic indices around mitochondria turnover, and finally post 28-day to check for long-term effect (Fig. 3.6) We observed an upward shift in OCR kinetics 2-day post-mitochondrial transplantation compared to the baseline (Figs. 3.5). Compared to the control, we observed a statistically significant improvement in basal respiration and ATP production 2-day post-transplantation ($p=0.031$ and $p=0.025$, respectively; Fig. 3.5). Maximal respiration and spare respiratory capacity—the cell's bioenergetics reserve in meeting a situation of high demand or

acute/chronic stress—were also enhanced post 2-day, although not statistically-significantly, p=0.060 for maximal respiration and p=0.080 for spare respiratory capacity (Fig. 3.5). Coupling efficiency was unchanged as both transplanted and native mitochondria were healthy (Fig. 3.5).

Mitochondrial superoxide production was measured 2-day post transplantation using MitoSOX Red in control and transplant groups, and no significant difference was observed among the groups (Fig. 3.7) [5].

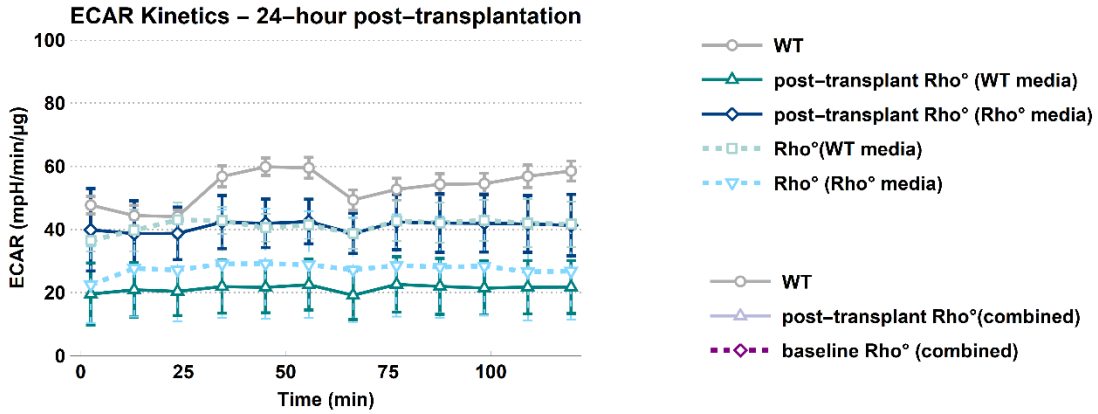
ECAR Kinetics – 24–hour post–transplantation
ECAR (mpH/min/µg)
Time (min)
WT
post–transplant Rho° (WT media)
post–transplant Rho° (Rho° media)
Rho°(WT media)
Rho° (Rho° media)
WT
post–transplant Rho°(combined)
baseline Rho° (combined)

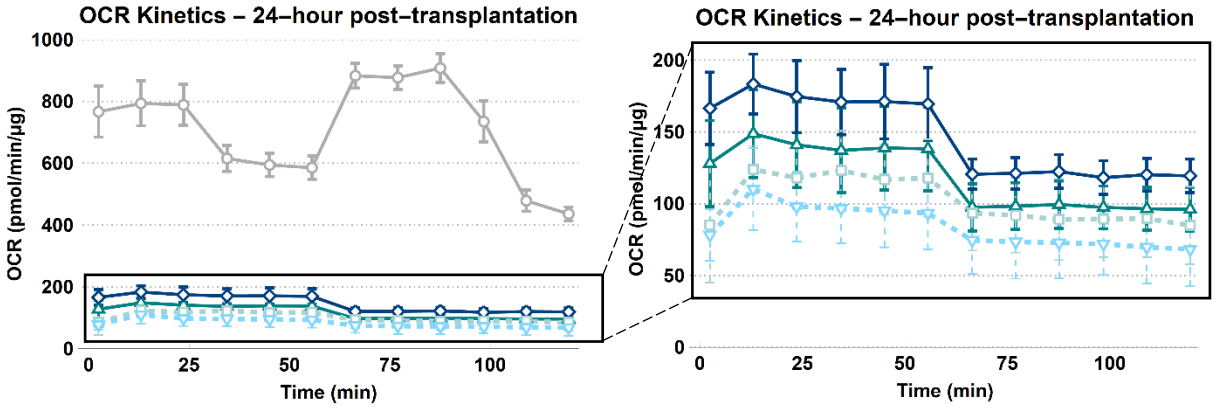
OCR Kinetics – 24–hour post–transplantation
OCR (pmol/min/µg)
Time (min)
OCR Kinetics – 24–hour post–transplantation
OCR (pmol/min/µg)
Time (min)

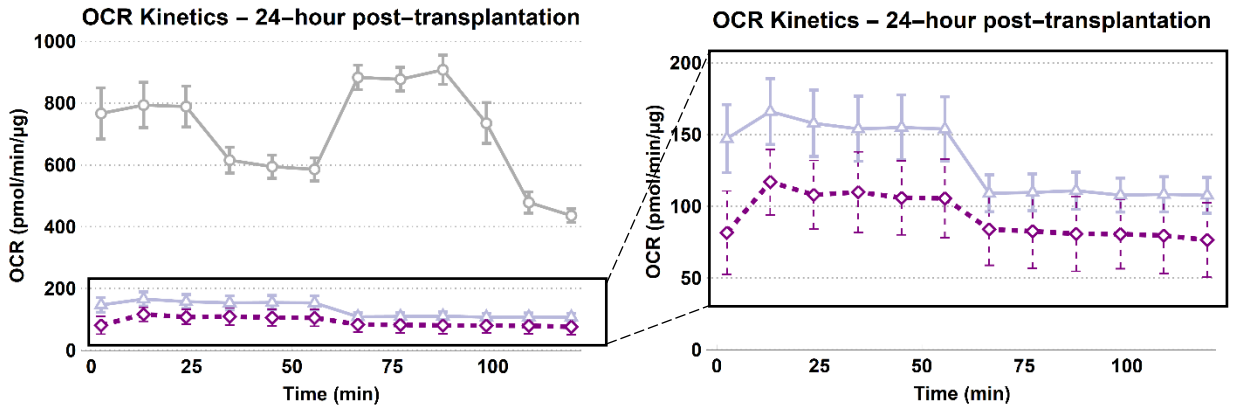
OCR Kinetics – 24–hour post–transplantation
OCR (pmol/min/µg)
Time (min)
OCR Kinetics – 24–hour post–transplantation
OCR (pmol/min/µg)
Time (min)

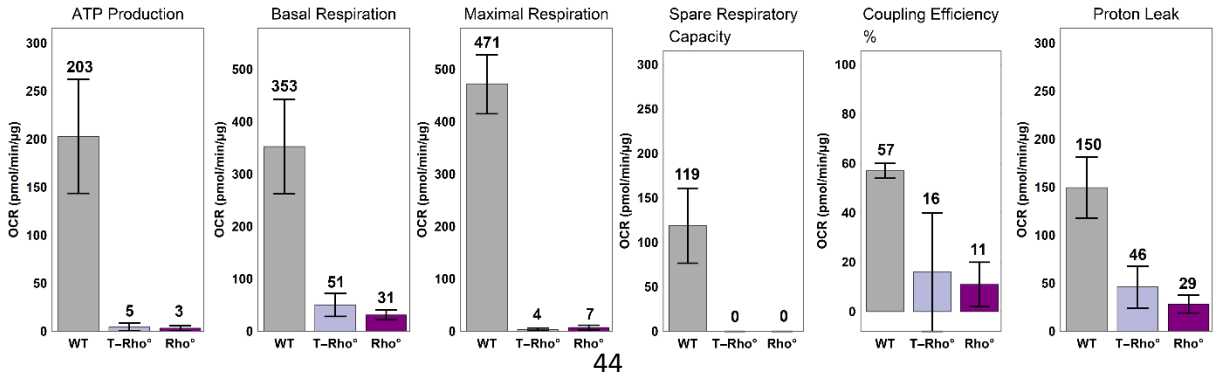
ATP Production
203
5
3
Basal Respiration
353
51
31
Maximal Respiration
471
4
7
Spare Respiratory Capacity
119
0
0
Coupling Efficiency %
57
16
11
Proton Leak
150
46
29
WT
T–Rho°
Rho°
OCR (pmol/min/µg)

Fig. 3.4 | Interspecies mitochondrial transplantation of rat L6 skeletal cells into ARPE-19 human retinal epithelial cells. Top. Extracellular Acidification Rate (ECAR) kinetics is relatively similar between post-transplanted rho zero, baseline rho zero, and wild type. Mitochondrial Transplantation (1:100 mitochondria: recipient cell) was not enough nor sufficient to restore mitochondrial function and bioenergetics in rho zero cells to that of the wild type. There was no significant difference between post-transplant rho zero cells that received the transplanted mitochondria in rho zero media (supplemented with uridine) vs. wildtype media lacking pyrimidine. **Bottom.** Post-transplant rho zero cells (lavender) more closely resemble the rho zero cells' kinetics (purple) than wild type (gray). Furthermore, the bioenergetics of post-transplanted rho zero is similar to that of the baseline rho zero cell. Basal respiration is increased in post-transplant rho zero cells, although not in a statistically significant manner. An unpaired two-tailed unequal variance student t-test was used and results with $p < 0.05$ were considered as statistically significant (n=8 for the combined post-transplant rho zero cells and n=8 for the combined rho zero cell and n=4 for the wild type group). Abbreviations: WT: Wild Type, T-Rho: Post-transplant Rho Zero cells

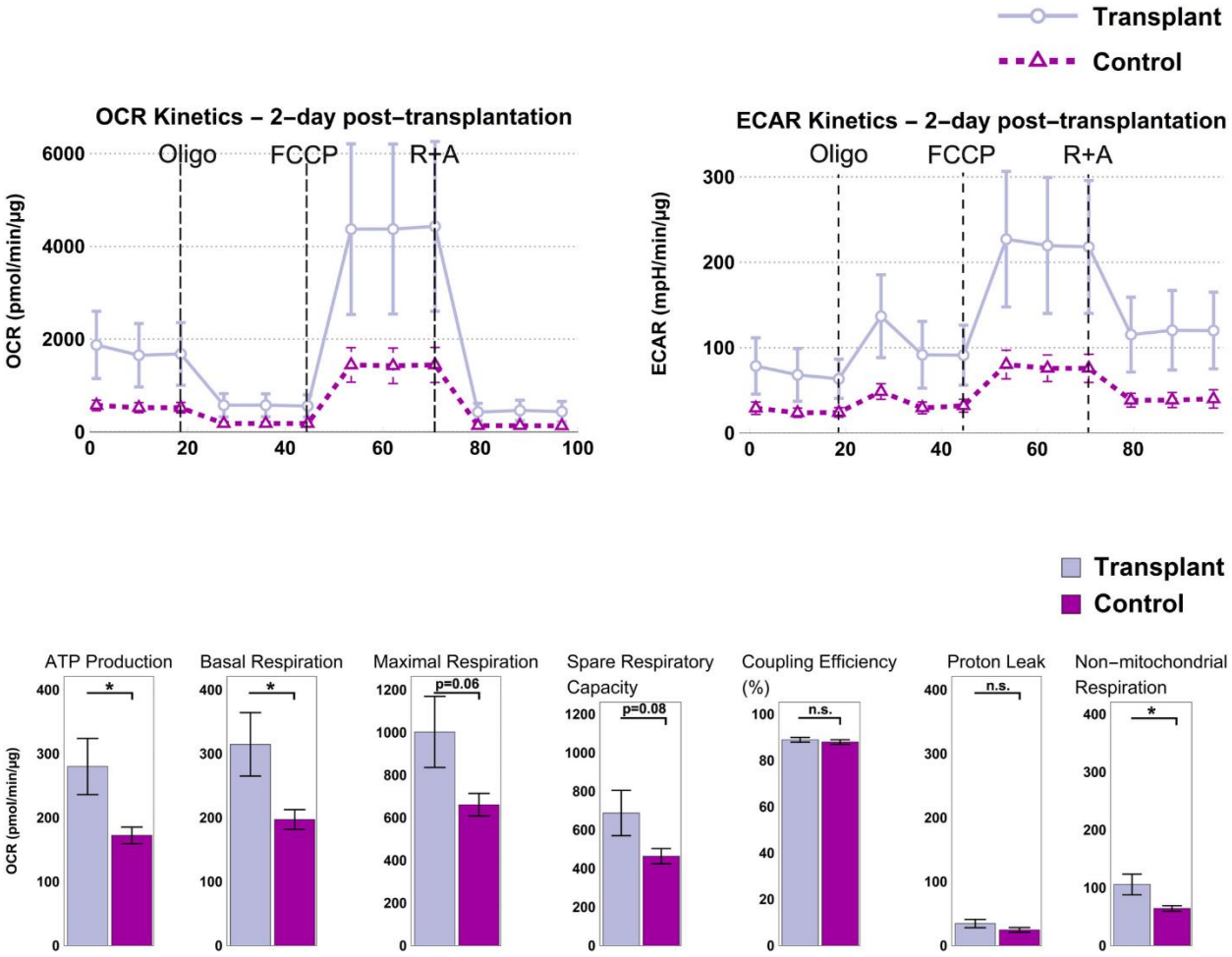

Fig. 3.5 | Non-autologous mitochondrial transplantation of L6 skeletal cells into H9c2 cardiomyocytes leads to enhanced bioenergetics 2-day post-transplantation. Top. Oxygen Consumption Rate (OCR) and Extracellular Acidification Rate (ECAR) kinetics increase 2-day post-transplantation indicating the improved metabolism after mitochondrial transplantation. Abbreviations: Oligo=Oligomycin; FCCP: carbonylcyanide-p-trifluoromethoxyphenyl hydrazine; R+A= Rotenone and Antimycin A. **Bottom.** Compared to control (lavender), there is a statistically significant increase in non-mitochondrial respiration, ATP production, and basal respiration in the transplant (purple) group. Maximal respiration and spare respiratory capacity are also enhanced, although not statistically significantly. Coupling efficiency and proton leak remain unchanged. An unpaired two-tailed unequal variance student t-test was used and results with $p < 0.05$ were considered as statistically significant (n=28 for transplant and n=12 for control) [5].

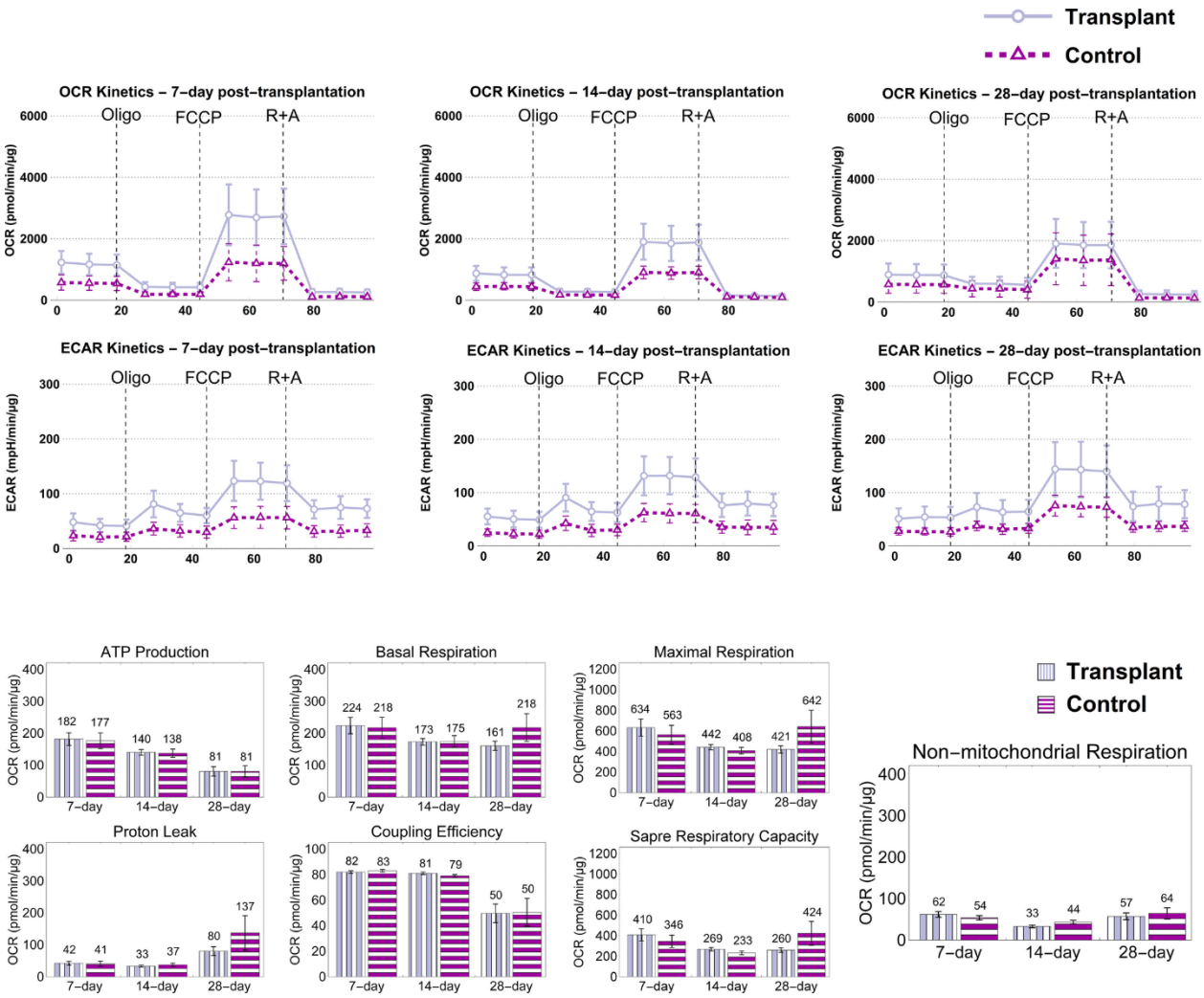

Fig. 3.6 | The acute enhancement in bioenergetics after mitochondrial transplantation diminishes in long-term. Top. No significant change in OCR and ECAR kinetics can be observed 7-day, 14-day and 28-day post-transplantation. Abbreviations: Oligo=Oligomycin; FCCP: carbonylcyanide-p-trifluoromethoxyphenyl hydrazine; R+A= Rotenone and Antimycin A. **Bottom.** No significant difference is found between the transplant (lavender) and control (purple) groups in long-term. While the bioenergetics return to the base-line levels in long-term, no negative consequences to the cell's bioenergetics was also observed due to the intervention. An unpaired two-tailed unequal variance student t-test was used and results with $p < 0.05$ were considered as statistically significant (n=28 for transplant and n=12 for control for t=7-day and 14-day, n=27 for transplant (due to well-measurement failure in one well) and n=12 for control for t=28-day)[5].

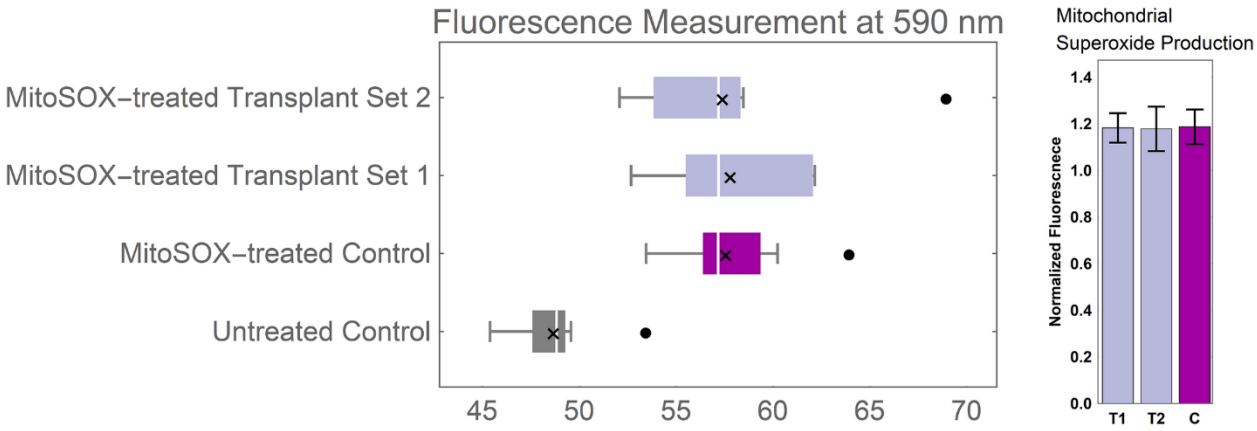

Fig. 3.7 | Mitochondrial superoxide production. 48-hour post mitochondrial transplantation, H9C2 cells were exposed to MitoSOX Red reagent to measure superoxide production. MitoSOX Red was excited at 485 nm and fluorescence emission was measured at 590 nm. The whisker box plot shows the distribution of the fluorescence readings for 10 measurements per group. Symbols: white line denotes the population median, "x" indicates the population mean, and filled black dots represent outliers. No statistically significant difference was observed in the population's mean of the post-transplant groups vs. control. The fluorescence measurements of MitoSOX-treated groups were normalized to the untreated control and displayed as bar graphs, for the mean ± SD [5].

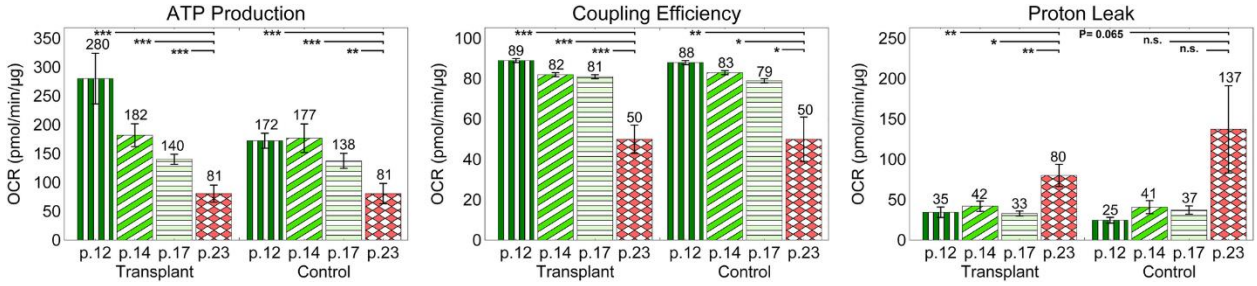

Fig. 3.8 | Effect of high passage number (aging) on mitochondrial function. Mitochondrial function was reduced with increasing passage number. This is indicated by the decrease in ATP production and coupling efficiency—positive indicators of mitochondrial function—and increase in proton leak— a negative indicator of mitochondrial function. An unpaired two-tailed unequal variance student t-test was used and results with $p < 0.05$ were considered as statistically significant (n=28 for p# 12, 14, and 17 and n=27 for p# 23 for transplant and n=12 for p# 12, 14, 17, and 23 for control) [5].

3. 4 DISCUSSION

As discussed in chapter 2, rho zero cells have mt-DNA defects that impair their oxidative phosphorylation and they rely on glycolysis for energy metabolism. We hypothesized and tested that through mitochondrial transplantation in ARPE-19 rho zero cells, the cells will adopt the mitochondria and in doing so oxidative phosphorylation will be restored (Fig. 3.4). Contrary to our belief, mitochondrial transplantation (at the attempted dosage) was not sufficient to restore oxidative phosphorylation. Although, oxygen consumption rate (OCR), representative of oxidative phosphorylation, increased in post-transplant rho zero cells vs. control rho zero cells, the overall profile resembled that of the rho zero cells and not that of the wild type. The extracellular acidification rate (ECAR), representative of glycolysis, remained relatively the same in wild type, rho zero and post-transplant rho zero. As discussed in chapter 2, while we had previously suspected that the environmental condition of the rho zero cells, at the time of transplantation might influence the success of transplantation and hence we had included two environmental conditions, where the uridine supplement needed for growth of rho zero cells were either removed at the time of transplantation or 24-hour after the transplantation, there was no significant difference between the two conditions and hence the two post-transplant rho zero cell groups and two rho zero cell groups were combined, irrespective of their media condition for the bioenergetics analysis (Fig. 3. 4) While the OCR kinetics increased, the changes in bioenergetics parameters in post-transplant rho zero cells were not statistically significant ($p > 0.05$) (Fig. 3.4). Additionally, the spare respiratory capacity revealed that rho zero cell's baseline respiration is already at its theoretical maximum and the cell's poor fitness, which is already known is due to the mtDNA defects in its electron transport chain.

H9c2 cells are phenotypically purely aerobic as the heart tissue has a high-energy demand, which is more efficiently met by aerobic respiration and oxidative phosphorylation. Increase in OCR kinetics 2-day post-transplantation is indicative of improved bioenergetics, which is justified by

more oxidative phosphorylation due to increased mitochondrial content (Fig. 3.5). Based on our bioenergetics results, it appears that in the normal cells, mitochondrial transplantation leads to acutely enhanced bioenergetics. However, these initial effects seem to diminish over time and return to that of the baseline control (Fig. 3.6).

In addition to OCR, we evaluated the ECAR from the Mito Stress Test (Fig. 3.5 and Fig. 3.6). In many cell types, mitochondrial activity (TCA cycle) that leads to CO_2 production is a significant source of extracellular acidification [34]. Since in our observation the ECAR significantly decreased after R+A injection, we suppose that in our samples the acidification was generated through the TCA cycle. However, from Mito Stress Test, only qualitative interpretation of the changes in ECAR data can be made for the kinetics after the injection of rotenone and antimycin. If the ECAR significantly decreases (i.e. low residual ECAR) in response to R+A, we infer the ECAR (prior to the injection of R+A) is primarily being generated via CO_2 production from the TCA cycle. If the ECAR remains constant and/or increases in response to R+A, then the ECAR prior to R+A treatment is primarily being generated via glycolysis [35]. It is also important to note that the exogenous pyruvate and glutamine supplemented in the media can be directly shunted into the TCA cycle, which lead to CO_2 production independent of the CO_2 produced from the pyruvate generated from glucose through glycolysis. Since we observed a decrease in response to R+A in both control and transplant groups, we infer that that CO_2 is primarily being generated via TCA cycle in this cell type. Another viewpoint indicates that in both control and transplant groups, the cells were burning through the exogenous pyruvate and glutamate. However, on the contrary, we interpret our ECAR data (Figs. 3.5 and 3.6), such that the increase in ECAR kinetics in transplant vs. the control group (Fig. 3.5) is due to CO_2 production from the increased TCA cycle in transplant group. Glycolytic Rate Assay can delineate the sole contribution of glycolysis or CO_2 to ECAR, which we did not perform in the current experiments [5].

Previously, Finck and Kelly [36], reported that the energetic needs of the cell finely tune the mitochondrial abundance, and too many or too few mitochondria may lead to pathology. In their review of myocardial energy metabolism, they associated myocardial diseases with perturbations of mitochondrial biogenesis. PGC-1α is a protein that drives mitochondrial biogenesis in cardiomyocytes by activating the nuclear respiratory factor 1, which in turn triggers the expression of activated mitochondria, leading to transcription and replication of the mitochondrial genome. Mice lacking PGC-1α present with signs of heart failure. Alternatively, downregulation of PGC-1α in mice leads to hypertrophic cardiomyopathy, whereas prolonged overexpression of PGC-1α in mice leads to increased biogenesis activity and mitochondrial ultrastructural abnormalities, which ultimately leads to death from heart failure [36]. Based on our observations, the enhanced bioenergetics state is temporary, which may imply that either the cells' mitochondrial content is returned to physiological levels, or the overall mitochondrial activities are reduced to reflect the cell's bioenergetics needs. Since the spare respiratory capacity, which measures the cell's capacity in meeting a situation of high energy demand, is not significantly changed in the transplant vs. the control, it is less likely that the overall mitochondrial activities have dampened and more likely that mitochondrial content has returned to physiological levels. Our observation corroborates with the findings of Finck and Kelly, and accordingly, we hypothesize that a normal cell clears any excess mitochondria keeping the mitochondrial content at physiological levels, as the plausible mechanism for the return of the bioenergetics indices to the baseline levels in long-term. In case of an adjustment of the mitochondrial content, it is yet unclear whether the newly transplanted mitochondria is cleared from the cell or if the transplanted mitochondria have been adopted by the host and the total mitochondrial level regardless of the recipient or donor status is reduced to bring the bioenergetics levels back to physiological state [5].

Moreover, the long-term bioenergetics profile suggests that there is no negative bioenergetic consequences due to mitochondrial transplantation and that the intervention can be considered

safe for the cell. The question remained to be answered is whether cells with damaged mitochondria would take advantage of the newly introduced mitochondria or not, as those cells could uptake and adopt the mitochondria differently than a normal cell, which is already able to efficiently meet its bioenergetics demands [5].

It is also important to note that non-mitochondrial respiration—an index that measures oxygen consumed by the cell via processes that are non-mitochondrial—significantly increased post 2-day ($p=0.033$) and returned to the baseline post 7-day, 14-day and 28-day ($p > 0.05$ for all; Fig. 3.5 and Fig. 3.6). Non-mitochondrial respiration is not well-understood or well-studied [37]. Some non-mitochondrial processes that use oxygen are superoxide production (with deleterious effects for mitochondria [38, 39]) and hydrogen peroxide production [40]. It is known that the hydrogen peroxide protects the cell from superoxide production given that it is properly degraded by catalase; otherwise it can break apart and form hydroxyl radicals. The increase in non-mitochondrial respiration could either suggest an improved overall metabolism or stress, which needs to be further investigated [5].

In a normal tightly coupled electron transport chain, approximately 1-3% of the consumed oxygen is incompletely reduced, which can lead to superoxide production as a result of the interaction between the leaky electrons and molecular oxygen.[41, 42] Since we had observed a statistically-significant enhancement in bioenergetics due to increased oxidative phosphorylation at 2-day post-transplantation, we used the mitochondrially-targeted derivative of hydroethidine (HE)—MitoSOX Red—to detect and quantitate the level of superoxide produced by mitochondria in post-transplant and control groups 2-day after transplantation. Compared to control, no statistically significant difference was found in superoxide production in the post-transplant group ($p=0.99$ and $p=0.83$ for set 1 and 2 transplantations, respectively; Fig. 3.7). The reported superoxide production was not assessed for the same Seahorse experiment, but a representative one.

Finally, we observed a reduction in mitochondrial function in the studied groups with increasing the passage number. ATP production and coupling efficiency, positive indicators of bioenergetics, significantly decreased with increasing passage number, while proton leak, a negative indicator of bioenergetics, significantly increased (Fig. 3.8) [5]. This observation corroborates with the findings of a previous study by Witek et al.[43], where they observed an increase in oxidative stress in cells with passaging of cardiomyocytes. It appears that mitochondrial function is reduced in cells with higher passage number and thus these cells are not representative of the initial passages. H9c2 cell-line is a well-established cell line used for assessing drug-induced cardiotoxicity [43] and this observation indicates that only lower passages of this line should be used to consider mitochondrial adverse events [5].

Limitations: Since the focus of the presented study has been on mitochondrial oxidative phosphorylation, Mito Stress Test was conducted. Thus, the ECAR kinetics presented in Figs. 3 and 4 represent the summation of acid (H^+) produced from glycolysis and CO_2 produced from the TCA cycle. Accordingly, the ECAR data in this study is not a direct measurement of glycolysis. The XF Glycolytic Rate Assay should be performed to quantitate the changes due to glycolysis.

CHAPTER 4: CURRENT WORKS AND SUMMARY

4.2 CURRENT WORKS

4.2.1 Assessment of mitochondrial genome post-transplantation. An unanswered question from our bioenergetics studies was whether mitochondria is adopted by the recipient cell in long-term

Table 4 | Description of Groups for Mitochondrial Genome Sequencing Studies Post Mitochondrial Transplantation

Group Descriptions

	Post-transplant	**Baseline**
1	Mitochondria from NHDF-Neo into Jurkat **(Non-autologous Human to Human Transplantation)**	NHDF only
2	Mitochondria from Jurkat into NHDF-Neo **(Non-autologous Human to Human Transplantation)**	Jurkat only
3	Mitochondria from NHDF-Neo into H9c2 **(Interspecies Human to Rat Transplantation)**	H9c2 only
4	Mitochondria from Jurkat into H9c2 **(Interspecies Human to Rat Transplantation)**	L6 only
5	Mitochondria from L6 into NHDF-Neo **(Interspecies Rat to Human Transplantation)**	
6	Mitochondria from L6 into Jurkat **(Interspecies Rat to Human Transplantation)**	

or cleared from the system. In order to answer this question as well as to answer whether a hybrid population of mitochondria can be formed from the fusion of transplanted mitochondria with the recipient cell's mitochondria, we decided to conduct a mitochondrial genome sequencing study post mitochondrial transplantation. The groups in this study are described in Table 4.

Mitochondrial DNA was extracted from cells using phenol chloroform extraction. To lyse the mitochondrial organelle and prepare the samples for extraction, 920 µL of DNA extraction buffer (10mM NaCL, 20 mM Tris-HCl, pH 8.0, 1 mM EDTA, prepared by combining 100 µL of 5 M NaCl, with 1 m: of 1M Tris-Hcl, pH 8.0, 100 µL of 0.5 M EDTA and water up to 50 mL) was added to the isolated mitochondrial pellet (mitochondrial organelle was isolated using ThermoFisher Scientific Kit). 50 µL of 10% SDS was added and mixed until the solution became viscous. Next, 30 µL of proteinase K solution was added, the 2.0 mL Eppendorf cap was closed tightly and mixed vigorously by vertexing. The tube was incubated at 55 °C for 3 hours, and gently inverted a few times every hour. The lysed sample is ready for the phenol extraction when it becomes viscous and relatively clear. An equal volume of equilibrated phenol was added and mixed gently by inversion for 1 minute, followed by centrifugation at 1,700 rcf at room temperature for 10 minutes. The upper clear aqueous layer was transferred to another tube very carefully to avoid carrying over phenol or white proteinaceous material from the interface. The phenol extraction was repeated once more. For the chloroform extraction, an equal volume of chloroform was added and mixed gently by inversion for 1 minute, followed by centrifugation at 1,700 rcf at room temperature for 10 minutes. The supernatant was transferred to another tube and the chloroform extraction was repeated for a second time to eliminate all of the phenol from the DNA sample. To purify the DNA 1/10th volume of 3 M sodium acetate (pH 5.2) was added and mixed well by vertexing, followed by adding 2x volume of ice-cold 100% ethanol. A white cotton-like precipitate forms upon doing this step. The tube was left in -20 °C overnight. The following day, the tube was

centrifuged at 14,000 rcf for 10 minutes at 4 °C. The pellet was rinsed with 70% ethanol, followed by letting it air-dry for about 15 minutes. The precipitate was dissolved in 100 µL of 10mM Tris. DNA yield and purity were determined with Nanodrop, by measuring the concentration to calculate the yield and assessing A260/A280 and A260/A230 to determine the purity. A260/A280 values were between 1.8 – 2.0 and A260/A230 were between 2.0 – 2.3, which indicated the purity of samples. Additionally, mt DNA size was checked by doing a gel electrophoresis and real-time PCR was performed to check for genomic contamination (Fig 4.2). We saw a band at the expected size of mitochondrial DNA, at ~16.5K and the mitochondrial DNA extract was free from genomic

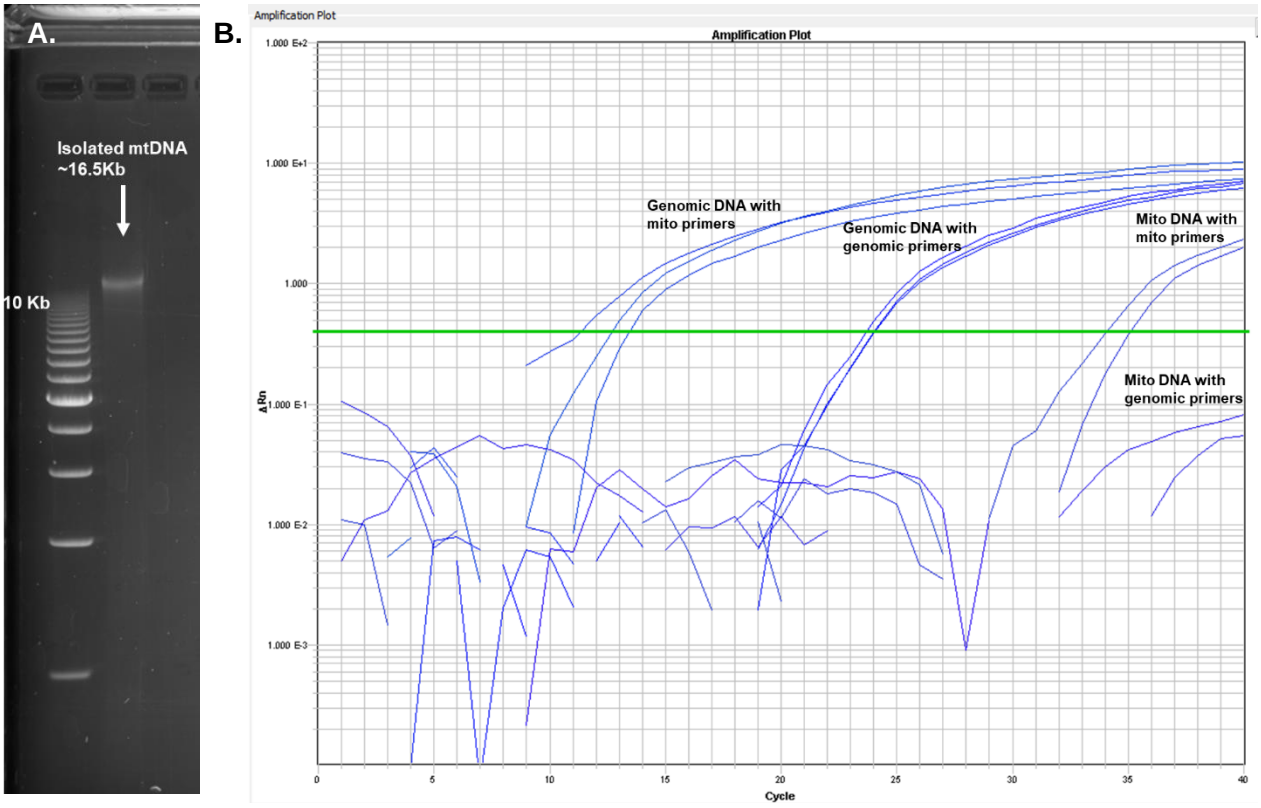

Fig. 4.1 | Purity of isolated mitochondrial DNA extracted via Phenol Chloroform extraction. A. Gel electrophoresis. reveals no genomic contamination, with a band appearing around 16Kb as expected. **B. Realtime PCR.** extracted mtDNA only amplifies with mitochondrial primers and not genomic primers, which confirms the isolated mitochondria is from genomic contamination.

contamination as the mitochondrial DNA did not amplify using genomic primers and only amplified in the presence of mitochondrial primers. The sequencing studies were abruptly interrupted by the campus closure caused by the COVID-19 and will be resumed when the campus re-opens.

4.2.2 Characterization of post-transplant mitochondrial morphology and dynamics using superresolution microscopy. A 12-hour super resolution time-lapse microscopy was conducted on a Nikon Yokogawa CSU-W1SoRa instrument. The images could not be analyzed due to the requirement of using IMARIS software available on the computers at the Optical Biology Core, which became unavailable as a result of the UCI campus closure caused by the COVID-19 pandemic and hence the result could not be included in this dissertation.

4.2 SUMMARY

In our studies, described in Fig. 4.1, we demonstrated the feasibility of autologous, non-autologous, and interspecies mitochondrial transplantation. More importantly, we showed that mitochondrial transplantation leads to transiently enhanced bioenergetics in normal cardiomyocytes, as evident by the statistically significant increase in the cells' basal respiration and ATP production. In our long-term post-transplantation studies, the bioenergetics returned to physiological levels in normal recipient cells and more studies are necessary to determine whether the outcome is different in cells with dysfunctional mitochondria. While, these enhancements are short-lived in normal cells, it is evident that there is also no adverse effects due to the transplantation, as the transplant cells are doing as well as the control cells in long-term, and there is no increase in mitochondrial superoxide production, which is a negative by-product of the oxidative phosphorylation.

This work delineates the potential of mitochondrial transplantation for clinical application in settings where there is an acute stress that would benefit from a boost in cellular bioenergetics. Given the observed bioenergetic profile of mitochondrial transplantation in normal cells, a remaining question would be if the post-transplantation bioenergetics profile will be any different in cells with mitochondrial dysfunction. These studies are crucial in determining the possible advantages of mitochondrial transplantation, if any, in mitigating mitochondrial diseases and other mitochondrial dysfunctions, as a cellular biotherapy.

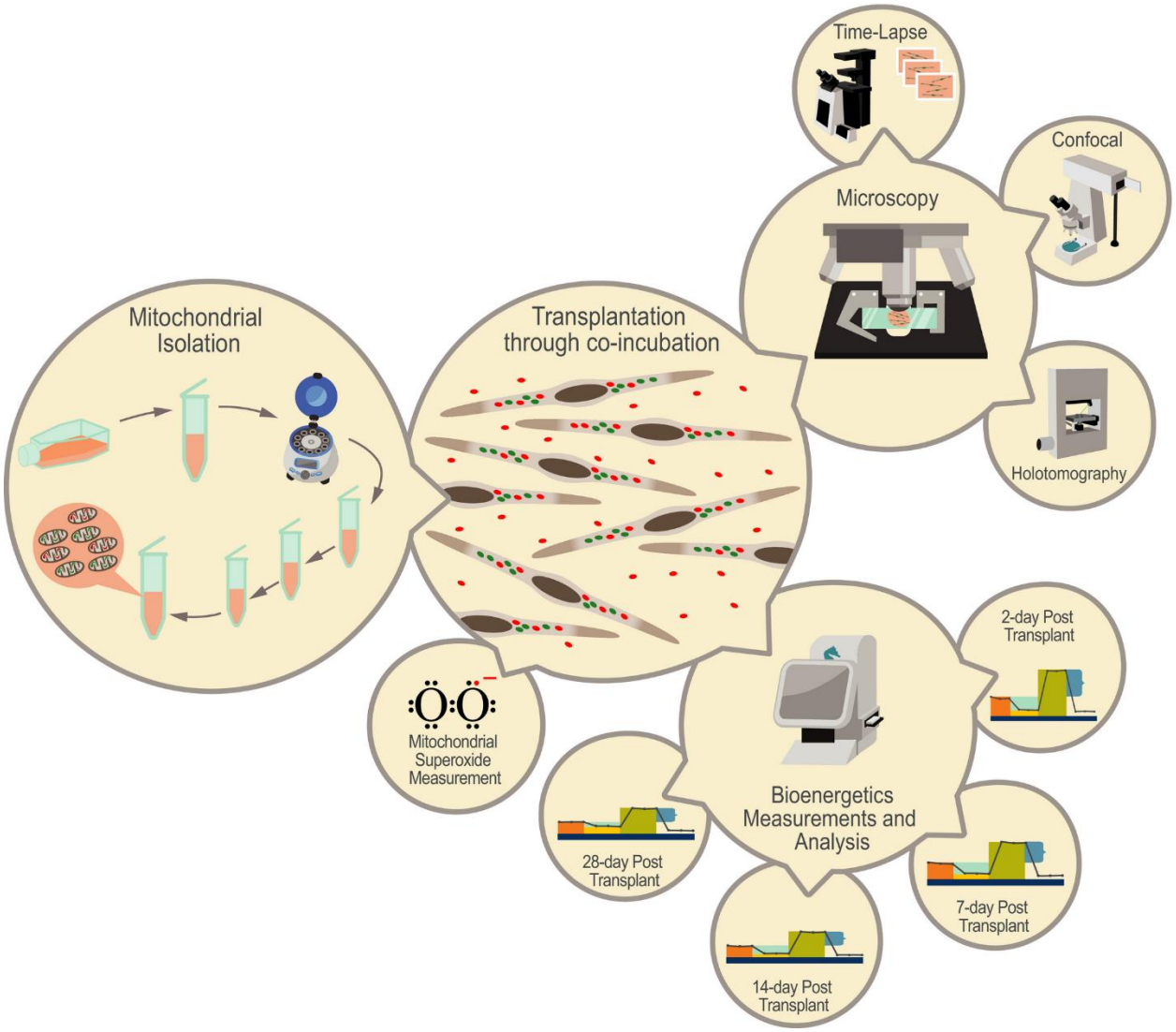

Fig. 4.2 | Mitochondrial transplantation studies in a glance. Feasibility of mitochondrial transplantation (autologous, non-autologous, and interspecies) was demonstrated using (a) widefield time-lapse, (b) confocal (c) holotomography microscopy and (d) superresolution microscopy. The bioenergetics consequences of non-autologous mitochondrial transplantation were studied using a Seahorse Flux Analyzer (a) 2-day, (b) 7-day, (c) 14-day, and (d) 28-day post transplantation. Mitochondrial superoxide was measured using MitoSOX Red Mitochondrial Superoxide Indicator (Mito-HE) [5].

CHAPTER 5: FUTURE DIRECTIONS AND CONCLUDING REMARKS

5.1 FUTURE DIRECTIONS

5.1.1 Bioenergetics and functional consequences of mitochondrial transplantation into neoplastic cells, immune cells, and cells from patients with mitochondrial disorders. A future direction of this work will be to investigate the bioenergetics changes due to mitochondrial transplantation in neoplastic cells such as cancer, immune cells such as T cells, and cells from patients with known mitochondrial disorders.

During the past decades, many approaches have been taken to eradicate the neoplastic cells. Classic chemotherapy agents, either alone or in combination with other drugs, target cells at different phases of the cell cycle: (1) *Alkylating agents* damage the neoplastic DNA; (2) *Antimetabolites* interfere with DNA and RNA by replicating RNA 'sand DNA's nucleotides; (3) *Anti-tumor antibiotics*, *Topoisomerase inhibitors*, and *Mitotic inhibitors* alter DNA inside the neoplastic cells to keep them from growing and multiplying. Newer approaches include: *Targeted chemotherapy* that takes advantage of differences between normal and neoplastic cells, and *Immunotherapy* that boosts or alter patient's immune system. However, to the best of our knowledge, improving T cell immune function through mitochondrial transplantation has not yet been attempted.

The theory of immune surveillance, introduced in early 1900s by Ehrlich, suggests that an intact immune system is essential to prevent the development and progression of neoplastic cells [44]. At the same it is known that cancer creates a suppressive metabolic microenvironment, which contributes to ineffective immune function [45]. In 1920s, Warburg postulated a hypothesis that suggested a defect in mitochondrial respiration as the ultimate cause of cancer. However, later research suggested that the metabolic shift from complete oxidation of glucose via oxidative

phosphorylation to incomplete conversion of glucose to lactate via glycolysis is linked to activation of oncogenes [46], and to the inactivation of tumor suppressor genes [47]. The metabolic changes of tumor itself causes a scarcity of glucose in the tumor microenvironment, where T cells directly complete for available glucose. As such T cells have a dynamic metabolic profile. Naïve T cells preferentially generate ATP through oxidative phosphorylation, while relying on glycolysis for activation, clonal expansion and effector function and need oxidative phosphorylation for survival and persistent antitumor response[48].

Scharping et al. have shown that the immunosuppressive tumor microenvironment leads to dysfunctional T cells with mitochondrial defects, characterized by an overall loss of mitochondrial mass, which consequently leads to defect in oxygen consumption and bioenergetics [49]. As such improving T cell mitochondrial function by increasing mitochondrial content via mitochondrial transplantation may restore the mitochondrial function in these cells and reduce the tumor burden by improving their antitumor response.

As a future direction, we will quantitate post-transplantation bioenergetics changes in T cells by measuring and comparing T cell's bioenergetic pre- and post- transplantation. More importantly, we will quantify post-transplantation immune response change compared to pre-transplantation by co-incubating the post-transplant T cells with cancer cell and assessing the cytokine levels from the supernatant via ELISA and cell-based flow cytometry cytotoxicity assay.

5.1.2 Assessment of calcium environment on transplanted mitochondria and mitochondrial transplantation. More recently, in an article published by Bertero et al.[50] in March 2020 and Chernyak [51] in April 2020, the effect of ca^{2+} on free mitochondria were described in a way that it may prevent the mitochondrial transfer to occur. They emphasized that this may happen *in presence of millimolar calcium concentrations*, because the isolated mitochondria may not tolerate an environment with high Ca^{2+} concentration. The scientists proposed that millimolar

calcium concentrations as in the blood, extracellular fluid, and typical *in vitro* conditions are beyond the buffering capacity of mitochondria and are toxic to them. Bertero and colleagues recently demonstrated the negative impact of calcium overload from culture medium on isolated mitochondria. Based on their findings, Bertero et al. suggested that mitochondria could only survive mitochondrial transplantation phenomenon observed by McCully et al. in presence of high Ca^{2+} concentration representative of the blood (and the in vitro conditions of our studies) if the Ca^{2+} is effluxed via the sodium-calcium exchanger, NCX. Blood's Ca^{2+} concentration is between 8.6 mg/dL to 10.3 mg/dL (2.15 mM – 2.57 mM) and in our *in vitro* studies the concentration of calcium present in cell culture media was at 1.8 mM. To test this hypothesis, Bertero et al. determined oxygen consumption and mitochondrial membrane potential by using the potentiometric dye tetramethylrhodamine methyl ester (TMRM), which is readily sequestered by active mitochondria and fluoresces red-orange. They tested isolated mitochondria in two environmental conditions, Ca^{2+}-free respiration buffer, or Tyrode solution with 1mM Ca^{2+} and 140 mM Na^{+}, and used ADP to induce respiration. They concluded that isolated skeletal muscle mitochondria are unable to withstand the environment of blood or the extracellular space, with millimolar concentrations of Ca^{2+}, because the depolarization of the mitochondrial membrane caused by the rapid calcium overload through the mitochondrial calcium uniporter (MCU), immediately and irreversibly damages the mitochondria [50]. In our opinion, their observation may not be attributed to mitochondrial transplantation because their experiments only considered isolated free mitochondria, while in the case of transplantation, most of these free-floating mitochondria are being transferred into the host cells at unknown rates. It is possible that the negative effect of Ca^{2+} on mitochondria would be transient, and if the mitochondria are taken by cells at a certain rate, they are not significantly affected. In our previous studies, we used DMEM media with high glucose and pyruvate (ThermoFisher Scientific, catalog number: 11995040), which has ~1.8mM of Calcium Chloride. However, we found through independent imaging studies

that the internalized mitochondria are dynamically repositioned (Figs. 2.2, 2.3, 2.7, 2.8, 2.9, 2.10, and 2.11), which may imply that they have survived. Additionally, the Seahorse flux analyzer results independently indicate a statistically significant improvement in basal respiration and ATP production 2 days post-transplantation ($p=0.031$ and $p=0.025$, respectively; Fig.3.5). Thus, the effect of Ca^{2+} on mitochondria in our experiments may be minimal or transient, may affect the transplant's efficiency by reducing the number of transferred mitochondria, or its isolated effects may be adjusted by other elements in the cell culture medium (e.g., sodium ions, etc.). If we find any of those to be true, we will consider using DMEM, high glucose, no glutamine, no calcium (ThermoFisher, catalog number: 21068028) instead.

In Chernyak's review, Chernyak discusses that there are numerous mechanisms controlling pore opening (for instance another known mechanism that can remove excess calcium ions and lower the calcium concentration relies on the plasma membrane Ca^{2+}-ATPse, PCMA); regardless, similar to Bertero et al., Chernyak also believes that these mechanisms would not prevent the pore opening at a ~ 1.8 mM concentration. Moreover, he argues that even if mitochondria do not undergo a full-scale swell, this concentration of calcium would lead to irreversible disruption of mitochondria because NAD/NADH, which normally allows for oxidation of the substrates at complex I of electron transport chain, would be washed out of the matrix. Regarding, Bertero et al.'s experiment, Chernyak suggests that unfortunately, since the authors did not experiment with blood serum, the experiment would not be sufficient to rule out that mitochondria can be saved in a high calcium concentration [51]. We agree with Chernyak that further experimentation is needed.

In our opinion, Bertero et al. observation may be biased because their experiments only considered isolated free mitochondria, which disregards the dynamics of the transplantation, while in the case of transplantation, most of these free-floating mitochondria are being transferred to

the host cells at unknown rates. It is possible that the negative effect of Ca^{2+} on mitochondria would be transient, and if the mitochondria are taken up by cells at a certain rate, they are not significantly affected. Moreover, in Bertero et al.'s experiment, isolated mitochondria were tested in Tyrode solution with 1 mM Ca^{2+} and 140 mM Na^{+}, and the effect of calcium concentration may be different in the DMEM solution that was used by us and independently other scientists[52, 53], or blood serum[54].

In our studies, isolated mitochondria in a DMEM environment were co-incubated with cells, which may change the outcome of the experiment. Given our microscopy observations using different imaging modalities (confocal, holotomagrpahy, and superresolution), short- and long- term transplantation bioenergetics, and independent use of DMEM by other scientists in mitochondrial transplantation/transfer studies [52, 53], it appears that functional mitochondria are in fact internalized by the cell.

As a future direction, given the significance of the ca2+ concentration as emphasized recently, it is necessary to design an experiment using both DMEM with calcium and without calcium in a parallel study of mitochondrial transplantation to determine how the calcium environment affects the mitochondria and mitochondrial transplantation efficiency and bioenergetics. Based on the observation of Bertero et al., we believe that mitochondrial transplantation efficiency may improve once the transplantation is attempted in a DMEM media with no calcium.

5.1.3 Mathematical modeling of the mitochondrial treatment. A mathematical program has been written in Mathematica, which may be used in future in conjunctions with the parameters gathered from the superresoultion time-lapse microscopy to simulate and test mitochondrial dynamics and the role of fission, fusion, biogenesis, mitophagy, and autophagy in mtDNA maintenance, and to also determine the dose and frequency of dose of mitochondrial transplantation treatment for varying degree of starting mtDNA mutation.

5.2 CONCLUDING REMARKS

This body of work contributes new knowledge to the field of mitochondrial engineering, which is a relatively new field concerned with novel treatments and therapies to mitigate mitochondrial disorders and dysfunction. There were a few numbers of mitochondrial transplantation attempts prior to this work; however, there was a limited understanding of the intracellular consequences of mitochondrial transplantation. Specifically, this work is the first to investigate the short- and long-term bioenergetics of mitochondrial transplantation. Our findings from non-autologous transplantation of skeletal muscle cell mitochondria into cardiomyocytes suggests that mitochondrial transplantation may hold a potential as a cellular biotherapy to be used in clinical settings where an acute boost of energy is needed by the cell and perhaps once the safety and efficacy is investigated in more depth, it may prove to be a useful treatment for mitochondrial disorders and dysfunctions.

Mitochondria are highly dynamic and undergo fusion, fission, and mitophagy to maintain a healthy network and to remove damaged mitochondria. We believe that by transplanting healthy mitochondria into a diseased cell, the cell can incorporate the normal mt-DNA and through the fusion of the new and old-damaged mt-DNA, followed by the fission of the mitochondria into healthy and damaged parts, clear the damaged mitochondria through mitophagy and reduce the mutation load. Investigating the cell's environment and responses post-transplantation will shed an understanding on whether mitochondrial transplantation holds promise as an effective cellular biotherapy for mitochondrial disease patients.

REFRENCES

1. Abcam. *Mitochondrial toxicity application guide*. 2016.
2. Abcam, *Mitochondrial dynamics, mitophagy, and autophagy.* 2018.
3. DiMauro, S., *Mitochondrial diseases.* Biochimica et Biophysica Acta (BBA) - Bioenergetics, 2004. **1658**(1): p. 80-88.
4. Chen, L., et al., *Advances in genome editing technology and its promising application in evolutionary and ecological studies.* GigaScience, 2014. **3**(1).
5. Ali Pour, P., M.C. Kenney, and A. Kheradvar, *Bioenergetics Consequences of Mitochondrial Transplantation in Cardiomyocytes.* Journal of the American Heart Association, 2020. **9**(7): p. e014501.
6. Agilent Technologies, *Multi-File XF Report Generator User Guide.* 2016.
7. Sebastian, D., M. Palacin, and A. Zorzano, *Mitochondrial Dynamics: Coupling Mitochondrial Fitness with Healthy Aging.* Trends Mol Med, 2017. **23**(3): p. 201-215.
8. Svensson, O.L., *Mitochondria : structure, functions, and dysfunctions.* 2010.
9. Wallace, D.C., *Why do we still have a maternally inherited mitochondrial DNA? Insights from evolutionary medicine.* (0066-4154 (Print)).
10. Seo, A.Y., et al., *New insights into the role of mitochondria in aging: mitochondrial dynamics and more.* Journal of Cell Science, 2010. **123**(15): p. 2533.
11. Schaefer, A.M., et al., *The epidemiology of mitochondrial disorders--past, present and future.* Biochim Biophys Acta, 2004. **1659**(2-3): p. 115-20.
12. El-Hattab, A.W. and F. Scaglia, *Mitochondrial Cardiomyopathies.* Front Cardiovasc Med, 2016. **3**: p. 25.
13. Elliott, R.L., X.P. Jiang, and J.F. Head, *Mitochondria organelle transplantation: introduction of normal epithelial mitochondria into human cancer cells inhibits proliferation and increases drug sensitivity.* Breast Cancer Research and Treatment, 2012. **136**(2): p. 347-354.
14. Zhang, J., et al., *Live birth derived from oocyte spindle transfer to prevent mitochondrial disease.* Reprod Biomed Online, 2017. **34**(4): p. 361-368.
15. Boominathan, A., et al., *Stable nuclear expression of ATP8 and ATP6 genes rescues a mtDNA Complex V null mutant.* Nucleic Acids Research, 2016. **44**(19): p. 9342-9357.
16. Gammage, P.A., et al., *Genome editing in mitochondria corrects a pathogenic mtDNA mutation in vivo.* Nature Medicine, 2018. **24**(11): p. 1691-1695.
17. Campbell, J.M., et al., *Engineering targeted deletions in the mitochondrial genome.* bioRxiv, 2018: p. 287342.
18. Moskowitzova, K., et al., *Mitochondrial transplantation prolongs cold ischemia time in murine heart transplantation.* J Heart Lung Transplant, 2019. **38**(1): p. 92-99.
19. Emani, S.M. and J.D. McCully, *Mitochondrial transplantation: applications for pediatric patients with congenital heart disease.* Transl Pediatr, 2018. **7**(2): p. 169-175.
20. Ramirez-Barbieri, G., et al., *Alloreactivity and allorecognition of syngeneic and allogeneic mitochondria.* Mitochondrion, 2018.
21. Cowan, D.B., et al., *Transit and integration of extracellular mitochondria in human heart cells.* Sci Rep, 2017. **7**(1): p. 17450.
22. Shin, B., et al., *Mitochondrial Transplantation in Myocardial Ischemia and Reperfusion Injury.* Adv Exp Med Biol, 2017. **982**: p. 595-619.
23. McCully, J.D., et al., *Mitochondrial transplantation: From animal models to clinical use in humans.* Mitochondrion, 2017. **34**: p. 127-134.

24. Emani, S.M., et al., *Autologous mitochondrial transplantation for dysfunction after ischemia-reperfusion injury.* The Journal of Thoracic and Cardiovascular Surgery, 2017. **154**(1): p. 286-289.
25. Kaza, A.K., et al., *Myocardial rescue with autologous mitochondrial transplantation in a porcine model of ischemia/reperfusion.* J Thorac Cardiovasc Surg, 2017. **153**(4): p. 934-943.
26. Cowan, D.B., et al., *Intracoronary Delivery of Mitochondria to the Ischemic Heart for Cardioprotection.* PLoS One, 2016. **11**(8): p. e0160889.
27. McCully, J.D., et al., *Mitochondrial transplantation for therapeutic use.* Clinical and Translational Medicine, 2016. **5**(1): p. 16.
28. Pacak, C.A., et al., *Actin-dependent mitochondrial internalization in cardiomyocytes: evidence for rescue of mitochondrial function.* Biology Open, 2015. **4**(5): p. 622.
29. Kitani, T., et al., *Internalization of isolated functional mitochondria: involvement of macropinocytosis.* Journal of Cellular and Molecular Medicine, 2014. **18**(8): p. 1694-1703.
30. Lee, S. and X. Chen, *Selective imaging of mitochondrial surfaces with novel fluorescent probes.* Chembiochem : a European journal of chemical biology, 2011. **12**(14): p. 2120-2121.
31. Banks, P.R. and D.M. Paquette, *Comparison of three common amine reactive fluorescent probes used for conjugation to biomolecules by capillary zone electrophoresis.* (1043-1802 (Print)).
32. Heller, S., et al., *Efficient repopulation of genetically derived rho zero cells with exogenous mitochondria.* PLoS One, 2013. **8**(9): p. e73207.
33. Lundholt, B.K., K.M. Scudder, and L. Pagliaro, *A simple technique for reducing edge effect in cell-based assays.* J Biomol Screen, 2003. **8**(5): p. 566-70.
34. Mookerjee, S.A., et al., *The contributions of respiration and glycolysis to extracellular acid production.* Biochimica et Biophysica Acta (BBA) - Bioenergetics, 2015. **1847**(2): p. 171-181.
35. Divakaruni, A.S., et al., *Chapter Sixteen - Analysis and Interpretation of Microplate-Based Oxygen Consumption and pH Data*, in *Methods in Enzymology*, A.N. Murphy and D.C. Chan, Editors. 2014, Academic Press. p. 309-354.
36. Finck, B.N. and D.P. Kelly, *Peroxisome proliferator-activated receptor gamma coactivator-1 (PGC-1) regulatory cascade in cardiac physiology and disease.* Circulation, 2007. **115**(19): p. 2540-8.
37. Hill, B.G., et al., *Integration of cellular bioenergetics with mitochondrial quality control and autophagy.* Biol Chem, 2012. **393**(12): p. 1485-1512.
38. Boveris, A. and B. Chance, *The mitochondrial generation of hydrogen peroxide. General properties and effect of hyperbaric oxygen.* Biochem J, 1973. **134**(3): p. 707-16.
39. Turrens, J.F., *Mitochondrial formation of reactive oxygen species.* J Physiol, 2003. **552**(Pt 2): p. 335-44.
40. Boveris, A., N. Oshino, and B. Chance, *The cellular production of hydrogen peroxide.* Biochem J, 1972. **128**(3): p. 617-30.
41. Jastroch, M., et al., *Mitochondrial proton and electron leaks.* Essays in biochemistry, 2010. **47**: p. 53-67.
42. Batandier, C., et al., *Determination of mitochondrial reactive oxygen species: methodological aspects.* Journal of Cellular and Molecular Medicine, 2002. **6**(2): p. 175-187.
43. Witek, P., et al., *The effect of a number of H9C2 rat cardiomyocytes passage on repeatability of cytotoxicity study results.* Cytotechnology, 2016. **68**(6): p. 2407-2415.
44. Töpfer, K., et al., *Tumor Evasion from T Cell Surveillance.* Journal of Biomedicine and Biotechnology, 2011. **2011**: p. 918471.
45. Levine, A.J. and A.M. Puzio-Kuter, *The control of the metabolic switch in cancers by oncogenes and tumor suppressor genes.* (1095-9203 (Electronic)).
46. Cairns, R.A., T.W. Harris Is Fau - Mak, and T.W. Mak, *Regulation of cancer cell metabolism.* (1474-1768 (Electronic)).

47. Le Bourgeois, T., et al., *Targeting T Cell Metabolism for Improvement of Cancer Immunotherapy.* Frontiers in oncology, 2018. **8**: p. 237-237.
48. Rivadeneira, D.B. and G.M. Delgoffe, *Antitumor T-cell Reconditioning: Improving Metabolic Fitness for Optimal Cancer Immunotherapy.* (1078-0432 (Print)).
49. Scharping, N.E., et al., *The Tumor Microenvironment Represses T Cell Mitochondrial Biogenesis to Drive Intratumoral T Cell Metabolic Insufficiency and Dysfunction.* Immunity, 2016. **45**(3): p. 701-703.
50. Bertero, E., B. O'Rourke, and C. Maack, *Mitochondria Do Not Survive Calcium Overload During Transplantation.* Circulation Research, 2020. **126**(6): p. 784-786.
51. Chernyak, B.V., *Mitochondrial Transplantation: A Critical Analysis.* Biochemistry (Moscow), 2020. **85**(5): p. 636-641.
52. Kitani, T., et al., *Internalization of isolated functional mitochondria: involvement of macropinocytosis.* (1582-4934 (Electronic)).
53. Kim, M.J., et al., *Delivery of exogenous mitochondria via centrifugation enhances cellular metabolic function.* Scientific Reports, 2018. **8**(1): p. 3330.
54. Masuzawa, A., et al., *Transplantation of autologously derived mitochondria protects the heart from ischemia-reperfusion injury.* American journal of physiology. Heart and circulatory physiology, 2013. **304**(7): p. H966-H982.